Reply on Referee Comment RC1 on acp-2021-52

In the following the comments of the referee are presented (in black) alongside with our replies (in blue) and changes made to the manuscript (in red).

General statement: The manuscript presents original and valuable experimental results accompanied by global model calculations. Furthermore, it is generally well written and presented. I suggest acceptance of the manuscript for publication, but I have a few minor comments to be considered before the final acceptance.

Dear reviewer, thank you very much for reviewing our manuscript and for the insightful comments. Below we provide detailed responses to your comments.

Comment 1: line 35: The wording "NOx is a toxic gas" sounds rather odd as NOx is not a single gas. To avoid misunderstandings the wording could be revised.

We have revised the sentence. It now says in line 35: Both NO and NO_2 are toxic gases which degrade surface air quality and regulate the abundance of secondary tropospheric oxidants.

Comment 2: line 41: The sentence needs revision.

We have revised the sentence. It now says: The U.S. Clean Air Act identified ozone as a criteria air pollutant in the 1970s (Jaffe et al., 2018).

Comment 3: line 84: You may also add some earlier references on NOx-VOC sensitivity of ozone production by Sillman.

We have added the already cited study of Sillman et al. "Photochemistry of ozone formation in Atlanta, GA – models and measurements" (1995) as a reference and another study by Sillman et al., "O_3-NO_x-VOC sensitivity and NO_x-VOC indicators in Paris: Results from models and Atmospheric Pollution Over the Paris Area (ESQUIF) measurements" to the list of references and as a reference to line 84: (Sillman et al., 1995; Sillman et al., 2003; Duncan et al., 2010, Nussbaumer and Cohen, 2020, Tadic et al., 2020).

Comment 4: lines 85-86: Please add a reference for the lifetime of NOx.

We have added a reference to lines 85-86 (Beirle et al., 2010).

Comment 5: There are a number of NOPR studies based on in situ HOx or ROx measurements by aircraft or at high altitudes stations which could be considered, e.g. Cantrell et al., 1996, Zanis et al., 2000, Cantrell et al., (2003a), Ren et al., (2008) Olson et al., (2012).

We have added Zanis et al. (2000a; The Role of In Situ Photochemistry in the Control of Ozone during Spring at the Jungfraujoch (3,580 m asl) – Comparison of Model Results with Measurements; https://doi.org/10.1023/A:1006349926926) and Cantrell et al. (2003; Peroxy radical behavior during the Transport and Chemical Evolution over the Pacific (TRACE-P) campaign as measured aboard the NASA P-3B aircraft; https://doi.org/10.1029/2003JD003674) to the list of references.

We have added the following sentence to the manuscript in line 367 (referencing Zanis et al., 2000a): The negative net ozone tendencies observed between 3 and 5 km altitude for the tropical troposphere stand in opposition to positive net ozone tendencies of about 0.1 ppbv h^{-1} (Zanis et al., 2000a) and balance in net ozone tendencies (NOPR ≈ 0) (HOOVER campaign over Europe; Bozem et al., 2017) deduced from previous measurements at similar altitudes at mid-latitudes.

We have added the following sentence to the manuscript in line 449 (referencing Cantrell et al., 2003): Especially the NO compensation mixing ratio (for which ozone production equals ozone loss) reproduces results from previous studies remarkably well. Cantrell et al. (2003) report NO compensation mixing ratios between 10 and 30 pptv over the Pacific, depending on whether modelled or measured HO_2 and RO_2 is used. A study conducted by Zanis et al. (2000b) for the Swiss Alps also reports balance in ozone production for similar NO compensation mixing ratios. Note that this second amendment addresses **Comment 17** of our reply. The respective reference (Zanis et al., 2000b) has been added to the list of references.

Comment 6: line 211: Should rather be "is practically one or unit" instead of unity.
We have revised line 211 accordingly.

Comment 7: line 211: Should be Tadic et al. (2017).
We have revised the passage accordingly.

Comment 8: line 235: You may also add some earlier references for the calculation of net ozone production (e.g. Lin et al., 1986).
We have added the suggested reference to the list of references and to line 235/236. However it should be Lin et al., 1988 (https://doi.org/10.1029/JD093iD12p15879) instead of 1986. We have further added Cantrell et al. (2003) as a reference for this sentence.

Comment 9: line 242-243: You may add a reference for the selection of the 100 ppbv criterion for stratospheric ozone. For example, see Prather et al., 2011. Other model intercomparison studies generally utilized a chemical tropopause defined at the 150 ppbv.
We have added Prather et al. (2011) to the list of references. Line 242ff now says (the underlined passage is new): Data are filtered for stratospheric influence by removing all data points for which concurrent O_3 is larger than 100 ppbv; a conservative criterion which has been discussed by Prather et al. (2011).

Comment 10: lines 251-253: The attribution of high NOx above 12 km to lightning NOx rather than NOx rich stratospheric air is rather speculative, unless if there are some indications from the model results of references for that. Mind also the simultaneous relatively smooth increase of both NO and O3 (as you also mention in page 10) which may point influence of stratospheric air.
Our argumentation is based the fact that the tropopause is located at about 16-18 km altitude at the ITCZ, which is still about 3-5 km above typical (highest) cruising altitudes of 12 – 14 km during the campaign. Second, although both NO and O3 show a slight increase above 12 km, the vertical CO profile shows only a slight decrease in average mixing ratios from about 100 ppbv around 12 km altitude to 80 ppbv around 15 km altitude which is statistically insignificant within $\pm$1 standard deviation of the vertical average CO mixing ratio. Assuming that stratospheric influence did play a (more) dominant role in terms of high NOx, the decrease in CO should be stronger than observed.
Also we have created two additional figures (added at the end of this reply) showing 2-D latitudinal/altitudinal distributions of measured, tropospheric NO and O3 during the campaign. Especially the latitudinal/altitudinal NO distribution shows rather local enhancements at the latitudinal range of the ITCZ than intrusion from the stratosphere at the subtropical jet streams.
We have further added these two figures discussed here to the supplement (as supplement Figure S5 and Figure S6) and redefined the numbering of the following supplement Figures accordingly. A short

passage has been added to the manuscript in line 343: Furthermore, supplementary Figures S5 and S6 show 2-D latitudinal-altitudinal distributions of measured, tropospheric NO and O_3, respectively.

Comment 11: line 264: At around 6 km it seems that there is an ozone layer of possible stratospheric origin. You may check this with relevant model diagnostics (e.g. specific humidity, potential vorticity or O3S if it is available from the simulation).
There is generally a lower data coverage for altitudes in the free and middle troposphere (between 4 and 10 km). The increase in modelled O3 at 6 km altitude arises from a few data points with increased mixing ratios at this altitude. A vertical profile of modelled humidity does not reproduce stratospheric influence.

Comment 12: lines 280-281: This does not necessarily mean that you totally exclude the influence of mixing with air of stratospheric origin.
No, we do not exclude mixing with air of stratospheric origin. To clearify this, we have added a short notice after the respective sentence in line 281f (underlined passage is new): We again remove stratospheric measurement data by only considering those for which O_3 was below 100 ppbv. Note that this does not necessarily exclude influence of mixing with air of stratospheric origin.

Comment 13: line 308: "…is shown.." should be deleted.
Thanks for noticing. We have removed "is shown" from the sentence.

Comment 14: line 368: Although the effect of humidity can be implied from factor α of Eq. 4 maybe it is also interesting adding in the supplementary material the observed and simulated specific humidity values.
We agree that is makes sense to add a comparison of the vertical profiles of observed and simulated humidity. We have added the following underlined sentence in line 349: We provide a vertical profile of α calculated based on Eq. 4, for which we obtain good agreement between measurements and simulations, for which we refer to the left graph of Figure S7 in the supplement. Supplementary Figure S7 also provides a comparison of vertical profiles of measured and simulated H_2O mixing ratios. The respective comparison of measured and modelled H2O mixing ratios has been added to supplement Figure S7 (which already shows the intercomparison of the vertical profile of α and $j(\mathrm{O1D})$). The revised Figure S7 (updated in the supplement) is included at the end of our reply.

Comment 15: line 379: Should rather be: "… is from a factor of 2-3 (below 3 km altitude) to a factor of 10 (above 12 km altitude) stronger …"
We have applied the suggested change.

Comment 16: Figure 7 is interesting showing the NO dependence of NORP as well as the ozone compensation point (the NO level at which NORP is roughly zero). One possibly limitation is the fact that the aggregated bins correspond to different atmospheric layers with different atmospheric characteristics which can possibly induce the spiky signal in the figure.
We agree that the spiky signature in the profile could be due to the variety of different air masses measured during the campaign and corresponding to a certain bin. We have added the following sentence to the passage below the figure (line 453ff): Note that one possible limitation of this figure arises from the fact that the data aggregated in the respective NO mixing ratio bins stem from different atmospheric layers and origins, which causes the spiky signature of the profile for both measurement and model.

Comment 17: line 441: You may also take into consideration the ozone compensation point which was derived in previous studies in the free troposphere and which agrees well with these values (see e.q. Zanis et al., JGR, 2000)

Zanis, P., Monks, P. S., Schuepbach, E., Carpenter, L. J., Green, T. J., Mills, G. P., Bauguitte, S., and Penkett, S. A.: In situ ozone production under free tropospheric conditions during FREETEX '98 in the Swiss Alps, J. Geophys. Res., 105, D19, https://doi.org/10.1029/2000JD900229, 2000b has been added to the list of references. **Comment 17** is being addressed within the answer to **comment 7**.

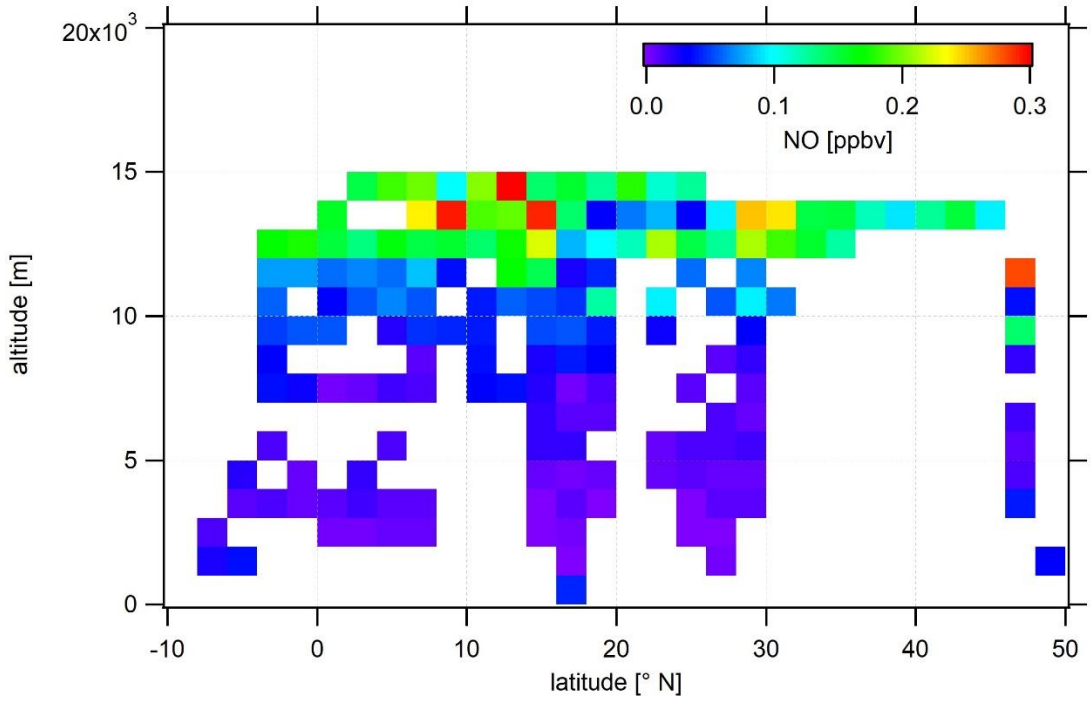

Figure S5: Latitudinal/altitudinal distribution of measured, tropospheric NO obtained during the campaign. The data have been aggregated and averaged over a grid width of 2 degree latitude and 1 km altitude.

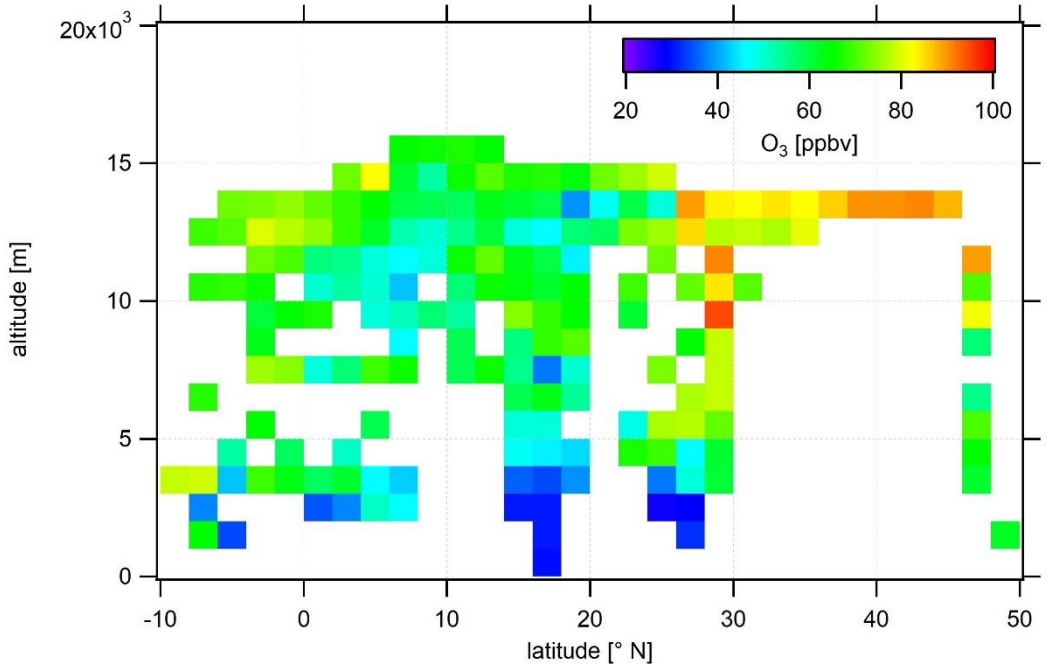

Figure S6: Latitudinal/altitudinal distribution of measured, tropospheric O_3 obtained during the campaign. The data have been aggregated and averaged over a grid width of 2 degree latitude and 1 km altitude.

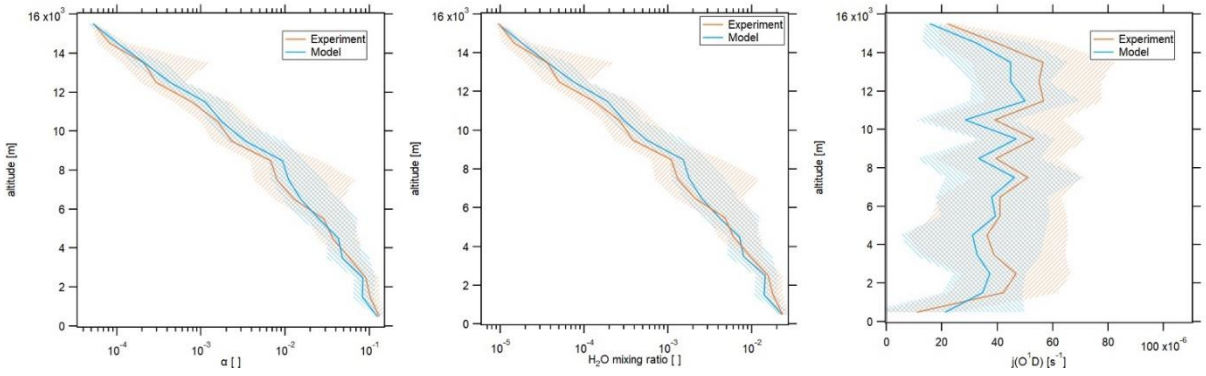

Figure S7: Vertical, tropospheric profile of α calculated based on measured and simulated data during CAFE-Africa (left graph). Vertical, tropospheric profile of H_2O mixing ratios calculated based on measured and simulated data during CAFE-Africa (middle graph). Vertical, tropospheric profile of $j(O^1D)$ (measured and simulated) obtained during CAFE-Africa (right graph). The orange and blue traces represent measured and simulated results, respectively.

Reply on Referee Comment RC2 on acp-2021-52

In the following the comments of the referee are presented (in black) alongside with our replies (in blue) and changes made to the manuscript (in red).

General description: The authors use aircraft observations of ozone and NO to estimate net ozone production rates in the upper troposphere over the Atlantic Ocean and West Africa. They determine that ozone production is NOx-limited. My recommendation is substantial changes to the manuscript before this should be considered for publication in ACP. These are detailed below.

Dear reviewer, thank you very much for reviewing our manuscript and for the insightful comments. Below we provide detailed responses to your comments.

General comments: The introduction does not provide the reader with context for what's known about the region and the time period sampled. The introduction details well-established ozone chemistry, rather than referring to prior publications that focus on ozone chemistry in the region. These include, but are not be limited to, publications that make use of observations from previous and ongoing flight campaigns in West Africa and over the Atlantic (AMMA, DACCIWA, MOZAIC, IAGOS, CARIBIC, ATom). URLs to some relevant publications are provided in the References section of this review. An introduction specific to the target region would clarify whether the finding in this study is in dispute, known already, or contrary to what's been found before.

Similarly, the results section should be compared to results published in the literature from previously published research.

We agree that it makes sense to provide the reader with information on ozone chemistry in the region by including observations from previous and ongoing flight campaigns. We have added a new paragraph to line 101ff (prior to the sentence "In the present study we characterize the distribution of NO and …):

A number of previous studies have performed measurements in the region of interest, the troposphere over the Atlantic Ocean and the West Africa (Lelieveld et al., 2004; Aghedo et al., 2007; Saunois et al., 2009; Real et al., 2010; Bourgeois et al., 2020). Lelieveld et al. (2004) indicated that positive ozone trends in the marine boundary layer over the Atlantic are likely caused by an increase in anthropogenic emissions of nitrogen oxides. Aghedo et al. (2007) showed that lightning acts as a major source of tropospheric NO_x, leading to a significant increase in middle and upper tropospheric ozone over the African continent. Saunois et al. (2009) described results from airborne measurements in the region during the AMMA project. Deploying a two-dimensional model for further analysis, Saunois et al. determined positive trends in photochemical net ozone production in the boundary layer over West Africa. There are also results from the ATom airborne mission, which measured vertical profiles of O_3 in the troposphere over the Atlantic Ocean (Bourgeois et al., 2020), which we will use to validate the results presented here. Real et al. (2010) investigated downwind O_3 production in pollution plumes in the mid and upper troposphere and determined mean net ozone production rates of 2.6 ppbv/day over a period of 10 days. However, studies reporting on vertical profiles and spatial distributions of nitric oxide, ozone and net ozone production rates as part of one coherent measurement project in the troposphere over the West African continent and the Atlantic Ocean are absent.

We added the here mentioned five studies to the list of references:

Aghedo, A. M., Schultz, M. G., and Rast, S.: The influence of African air pollution on regional and global tropospheric ozone, *Atmos. Chem. Phys.*, **7**, 1193-1212, https://doi.org/ 10.5194/acp-7-1193-2007, 2007.

Bourgeois, I., Peischl, J., Thompson, C. R., Aikin, K. C., Campos, T., Clark, H., Commane, R., Daube, B., Diskin, G. W., Elkins, J. W., Gao, R.-S., Gaudel, A., Hintsa, E. J., Johnson, B. J., Kivi, R., McKain, K., Moore, F. L., Parrish, D. D., Querel, R., Ray, E., Sánchez, R., Sweeney, C., Tarasick, D. W., Thompson, A. M., Thouret, V., Witte, J. C., Wofsy, S. C., and Ryerson, T. B.: Global-scale distribution of ozone in the remote troposphere from the ATom and HIPPO airborne field missions, *Atmos. Chem. Phys.*, **20**, 10611–10635, https://doi.org/10.5194/acp-20-10611-2020, 2020.

Lelieveld, J., van Aardenne, J., Fischer, H., de Reus, M., Williams, J., and Winkler, P.: Increasing Ozone over the Atlantic Ocean, *Science*, **304**, Issue 5676, 1483-1487, https://doi.org/10.1126/science.1096777, 2004.

Real, E., Orlandi, E., Law, K. S., Fierli, F., Josset, D., Cairo, F., Schlager, H., Borrmann, S., Kunkel, D., Volk, C. M., McQuaid, J. B., Stewart, D. J., Lee, J., Lewis, A. C., Hopkins, J. R., Ravegnani, F., Ulanovski, A., and Liousse, C.: Cross-hemispheric transport of central African biomass burning pollutants: implications for downwind ozone production, *Atmos. Chem. Phys.*, **10**, 3027–3046, https://doi.org/10.5194/acp-10-3027-2010, 2010.

Saunois, M., Reeves, C. E., Mari, C. H., Murphy, J. G., Stewart, D. J., Mills, G. P., Oram, D. E., and Purvis, R. M.: Factors controlling the distribution of ozone in the West African lower troposphere during the AMMA (African Monsoon Multidisciplinary Analysis) wet season campaign, *Atmos. Chem. Phys.*, **9**, 6135-6155, https://doi.org/10.5194/acp-9-6135-2009, 2009.

A discussion of the O_3 vertical profile with respect to results from the ATom mission has been included in the manuscript in line 300ff:

O_3 profiles observed in this study are in good agreement with results from the ATom mission (Bourgeois et al., 2020). For the June-August season, Bourgeois et al. show that in the tropical troposphere O_3 increased with altitude to 50 ppbv at 5-6 km whereas above 9 km O_3 varied from 40 to 80 ppbv, supporting the results presented here (see Figures 9 and 10 in Bourgeois et al., 2020).

Another section has been added to discuss the relevance of photochemical ozone production derived in this study in line 437:

Our results add to the understanding of photochemical net ozone production in the upper troposphere of the region. Using a photochemical trajectory model initiated by in situ measurements, Real et al. (2010) derived photochemical net ozone production rates of 2.6 ppbv/day over a period of 10 days downwind of West Africa. Our study supports the findings by Real et al. (2010) by underlining that photochemical ozone production in the upper troposphere over the tropics is positive at about 0.2-0.4 ppbv h^{-1}, which supports the concept of significant photochemical ozone production in the upper troposphere of the region. Note that during CAFE-Africa, measurements at low altitudes were generally performed over the Atlantic Ocean. Hence we cannot compare to previous results from Saunois et al. (2009) reporting ozone production ranging from 0.25 to 0.75 ppbv h^{-1} in the continental boundary layer over West Africa (2009).

The measurement techniques the researchers use are established techniques, so instead dedicate the methods section to describing the aspects of these that are unique and relevant to your study.
We consider the section describing the measurement methods and techniques to be essential to the study. We have added a short sentence in line 197 emphasizing the applicability of the instrumental set up for observations on an airborne platform:
All instruments deployed on the aircraft have been developed to meet the high standards of airborne measurements in terms of operability, accuracy and sensitivity.

Avoid unfamiliar and unnecessary acronyms when there are mathematical symbols or familiar letters that would be easier for the reader to follow. NOPR, RMU, and TMU are not universally familiar. For NOPR, for example, consider rather using P(O3)net. P(O3)gross could then be used to distinguish the two. Many acronyms in the paragraph starting on line 111 seem unnecessary and make it a challenge to read.
We agree that it makes sense to unify "total measurement uncertainty" (TMU) and "relative measurement uncertainty" (RMU), which describe in principle the same phenomenon. We have therefore replaced "relative measurement uncertainty"/"RMU" in Table 1 and in the caption of Table 1 by "total measurement uncertainty"/"TMU".
However, in terms of the acronym NOPR we have to state that the acronym/symbol for net ozone production rate" is not unified in the community. Previous studies (Thornton et al., 2002) used the acrnonym "$P(O_3)$" as the gross rate of O_3 production, which is equivalent to what is given in our study. Also Real et al. (2010, https://doi.org/10.5194/acp-10-3027-2010) abbreviated "net ozone production" by "NPO_3", similar to the acronym "NOPR" mentioned in our study. Last but not least, "NOPR" has already been established in previous studies (Bozem et al., 2017; Tadic et al., 2020). We would like stay with the used acronym "NOPR".
Nevertheless to make it easier to follow the manuscript, we have added short notices in line 231: Note that other studies use $P(O_3)$gross as an acronym for $P(O_3)$ in Eq. 2.
… and in line 238:
Note that other studies use P(O3)net as an acronym for NOPR in Eq. 6.

Comment 1: Line 118: How does the flight ceiling compare to the tropopause height during the flight campaign?
The tropopause is located at about 16-18 km altitude at the ITCZ, which is 3-5 km above the flight ceiling. At higher latitudes (~ 30° N), the tropopause is located at about 13-15 km.

Comment 2: Figure 1 caption: Provide dates instead of flight numbers. The former are more meaningful.
We have replaced the flight numbers by flight dates. A revised version of Figure 1 (with revised caption) can be found at the end of this document. We have revised lines 128ff in the manuscript (underlined words are new) to facilitate the attribution of flight dates to flight numbers: For the analysis of the MFs, we consecutively numerate each MF. We start with MF03 <u>on August 07, 2018</u> for the ferry flight from Oberpfaffenhofen (Germany, Deutsches Zentrum für Luft- und Raumfahrt) to Sal (Cape Verde Islands) and ending with MF16 <u>on September 07, 2018</u> for the back ferry flight from Sal to Oberpfaffenhofen.

Comment 3: What does the model simulate? Global?
Yes, EMAC is a global model. We have clarified this at the beginning of chapter 2.4 by adding the attribute "global" to the description of EMAC (underlined word is new): EMAC is a 3-D <u>global</u> general

circulation, atmospheric chemistry-climate model, which has been used and described in a number of previous studies (Roeckner et al., 2006; Jöckel et al., 2016; Sander et al., 2019; Tadic et al., 2020).

Comment 4: Are soil NOx emissions in the model? If so, give the name and reference of the inventory. If not, would this contribute to the model-measurement discrepancy in NO in the lower troposphere?
NOx soil emissions are included in the model. However, there is no inventory itself in the model as NOx soil emissions are calculated online by an algorithm described by Yienger and Levy II (Yienger and Levy II, 1995; Kerkweg et al., 2006). Based on the Yienger and Levy II algorithm, Pozzer et al. have determined a yearly emission of NOx at 6.77 to 7 TgN/yr (see supplement of Pozzer et al., 2007). Weng et al. found that averaged over the last 37 years, global total soil NOx emissions amount to 9.5 TgN/yr (2020), which means that NOx soil emission in the EMAC model might be on the lower end of the most recent estimates. We have added the following sentence to the description of the model in line 216: The NO_x soil biogenic emission flux is calculated based on a semi-empirical emission algorithm implementation by Yienger and Levy II (1995; Kerkweg et al., 2006).
Yienger and Levy II (1995) has been added to references of the manuscript. Kerkweg et al. is already cited in the manuscript.

Yienger, J. and Levy II, H.: Empirical model of global soil-biogenic NO_x emissions, *J. Geophys. Res.*, **100**, 11 447–11 464, https://doi.org/10.1029/95JD00370, 1995.

Pozzer et al.: Simulating organic species with the global atmospheric chemistry general circulation model ECHAM5/MESSy1: a comparison of model results with observations, *Atmos. Chem. Phys.*, **7**, 2527–2550, 2007.

Weng et al.: Global high-resolution emissions of soil NO_x, sea salt aerosols, and biogenic volatile organic compounds, *Sci Data*, **7**, 148 (2020).

Comment 5: Line 198: What is “tg”? Do you mean “Tg”?
Yes, we mean “Tg”. We have revised the unit accordingly (now line 214)

Comment 6: Line 211: Format of the in-text citation of Tadic et al. is incorrect.
We have revised the passage accordingly.

Comment 7: Line 213: What does “Therewith” mean? Is it necessary?
We agree that “therewith” is redundant. We have removed “therewith” from the sentence.

Comment 8: Line 217-221: This is a very lengthy sentence that makes for challenging reading.
We agree that it makes sense to rewrite this sentence. We have also clarified the acronym PSS in line 219 (which addresses comment 9). Line 236ff now say: We further assume photostationary steady state (PSS) for the probed air masses. As the typical time to acquire PSS during CAFE-Africa varied between 40 s at 2 km altitude and about 70-80 s at 15 km altitude (Mannschreck et al., 2004; Tadic et al., 2020), we can calculate the concentration of CH_3O_2 by the equation derived by Bozem et al. (2017).

Comment 9: Line 219: Tell the reader what “PSS” is.
See answer to comment 8.

Comment 10: Lines 225-226: The dominant loss pathway for HCHO leading to the formation of HO2 is photolysis. If this loss pathway is also taken into account, is HO2 production from HCHO still negligible?
In the manuscript we have conservatively estimated ambient HCHO mixing ratios at 100 pptv, which represents an upper limit for HCHO and is most likely a factor of 2 too high. Taking into account the photolysis of HCHO (being an additional pathway of HO2 production) results in HO2 production from the reaction of CO with OH being on average a factor of 5 larger than the sum of HO2 production from the sum of the reaction of H2 with OH, the reaction of HCHO with OH and photolysis of HCHO. In combination with the fact that 100 pptv already represents an upper limit for HCHO, we still can assume that the reaction of CO with OH dominates HO2 production during most of the campaign time to estimate CH3O2. Nevertheless, we have incorporated this new finding into the manuscript in line 241ff: Note that the reaction of CO with OH represents the dominant term in HO2 production during CAFE-Africa. Assuming mixing ratios of 500 ppbv and 100 pptv for H2 and HCHO, respectively, we find that HO2 production rate from the reaction of OH with CO is on average 5 times greater than the sum of the HO2 production rates from photolysis of HCHO and the reactions of HCHO and H2 with OH during CAFE-Africa. Note that the assumed mixing ratio of 100 pptv represents a rather conservative upper estimate for HCHO in the upper troposphere.

Comment 11: Equation (6): Is the righthand side of this equation just "$P(O_3)$gross – $L(O_3)$"? If so, consider rewriting it to this so that it is clearer that this relates to what's given in equations (2) and (5).
Yes, the righthand side of this equation is just "$P(O_3)$gross – $L(O_3)$". Equation 6 now reads as:

$$\mathrm{NOPR} = P(\mathrm{O_3}) - L(\mathrm{O_3}) =$$
$$[\mathrm{NO}] \cdot \left(k_{\mathrm{NO+HO_2}}[\mathrm{HO_2}] + k_{\mathrm{NO+CH_3O_2}}[\mathrm{CH_3O_2}]\right) - [\mathrm{O_3}] \cdot (\alpha \cdot j(\mathrm{O^1D}) + k_{\mathrm{OH+O_3}}[\mathrm{OH}] + k_{\mathrm{HO_2+O_3}}[\mathrm{HO_2}])$$

Comment 12: Lines 231: It's not clear whether the quoted values are calculated in this work or are from a previous study. Rewrite for clarity.
These values represent results from a previous study (Bozem et al., 2017). We have clarified this by revising line 251: In the troposphere, α ranges from about 15 % in the PBL to 1 % in the upper troposphere, where absolute humidity is very low (Bozem et al., 2017).

Comment 13: Figure 2: Considering the simulated NO variability extends into the negative, provide the min and max values of the modelled and observed NO.
The simulated NO variability extends into the negative due to the large variability of NO data at highest altitudes. Note that the model itself does not yield any negative data at all. However having a few simulated data points with large NO mixing ratios results in a relatively large standard deviation of the respective average and, consequently, in the variability ($\pm$ 1 standard deviation) being negative above 12 km altitude. The min and max mixing ratios of modelled NO are zero and 2.13 ppbv, respectively. The mix and max mixing ratios of observed NO are zero and 0.95 ppbv. This finding has been incorporated into the study in line 284: The minimum and maximum mixing ratios of modelled NO are zero and 2.13 ppbv, respectively. The minimum and maximum mixing ratios of observed NO are zero and 0.95 ppbv, respectively.

Comment 14: Lines 252-253: Why would there be influence from the stratosphere if this has been removed using an ozone concentration threshold?

The ozone mixing ratio threshold of 100 ppbv only removes measurements obtained directly in the stratosphere where O3 significantly exceeds 100 ppbv. However, this threshold does not remove all periods with stratospheric influence. Take for instance an (upper) tropospheric air mass with intrinsically low O_3. Influence from the stratosphere could result in an increase in O_3 which however would not necessarily result in O_3 mixing ratios larger than 100 ppbv.

Comment 15: Line 309: Avoid subjective words like "interestingly".
We have removed "interestingly" from this sentence.

Comment 16: Line 433: Change "Please note that there …" to "There …".
We have revised line 474 accordingly. It now says: ~~Please note that~~ There is only limited data coverage for measured NO above 0.325 ppbv and for simulated NO above 0.15 ppbv. See supplementary table ST3 for the number of data points in each NO mixing ratio bin.
The second sentence of this amendment already addresses comment 18 (to add the number of data points in each NO concentration bin.).

Comment 17: Line 432: Was there any doubt or contention that the upper troposphere is NO_x-limited over this region?
There was no doubt or contention that the upper troposphere might or might not be NO_x-limited. This is a fundamental finding, which arises from the dependency of net ozone production on NO (presented in Figure 7), which has, as far as we know, not been presented before for the upper troposphere over the Atlantic Ocean and West Africa.

Comment 18: Give the number of data points in each NO concentration bin.
The number of data points in each NO concentration bin are given in the following table, which has been added to the supplements of this study. We have further revised sentence in Line 474ff: There is only limited data coverage for measured NO above 0.325 ppbv and for simulated NO above 0.15 ppbv. See supplementary table ST3 for the number of data points in each NO mixing ratio bin.

Table ST3: Number of data points in each NO mixing ratio bin. Note that the data coverage of the simulation is larger than that of the measurement due to gaps in the observational data.

NO mixing ratio bin	measurement	simulation
0 pptv ≤ NO < 25 pptv	140	226
25 pptv ≤ NO < 50 pptv	54	70
50 pptv ≤ NO < 75 pptv	36	40
75 pptv ≤ NO < 100 pptv	23	60
100 pptv ≤ NO < 125 pptv	50	38
125 pptv ≤ NO < 150 pptv	44	24
150 pptv ≤ NO < 175 pptv	28	7
175 pptv ≤ NO < 200 pptv	30	7

200 pptv ≤ NO < 225 pptv	21	3
225 pptv ≤ NO < 250 pptv	15	7
250 pptv ≤ NO < 275 pptv	11	3
275 pptv ≤ NO < 300 pptv	12	5
300 pptv ≤ NO < 325 pptv	11	5
325 pptv ≤ NO < 350 pptv	3	3
350 pptv ≤ NO < 375 pptv	2	6
375 pptv ≤ NO < 400 pptv	3	2
400 pptv ≤ NO < 425 pptv	1	1
425 pptv ≤ NO < 450 pptv	5	2
450 pptv ≤ NO < 475 pptv	1	3
475 pptv ≤ NO < 500 pptv	1	3

Comment 19: Lines 445: Should “tropical troposphere” be “upper troposphere in the tropics”, as this is the focus of the study according to the title.

We have revised lines 445 and 446 accordingly. It now says in line 492ff: However, both model simulations and observations indicate that O_3 production in the upper troposphere in the tropics is NO_x-limited.

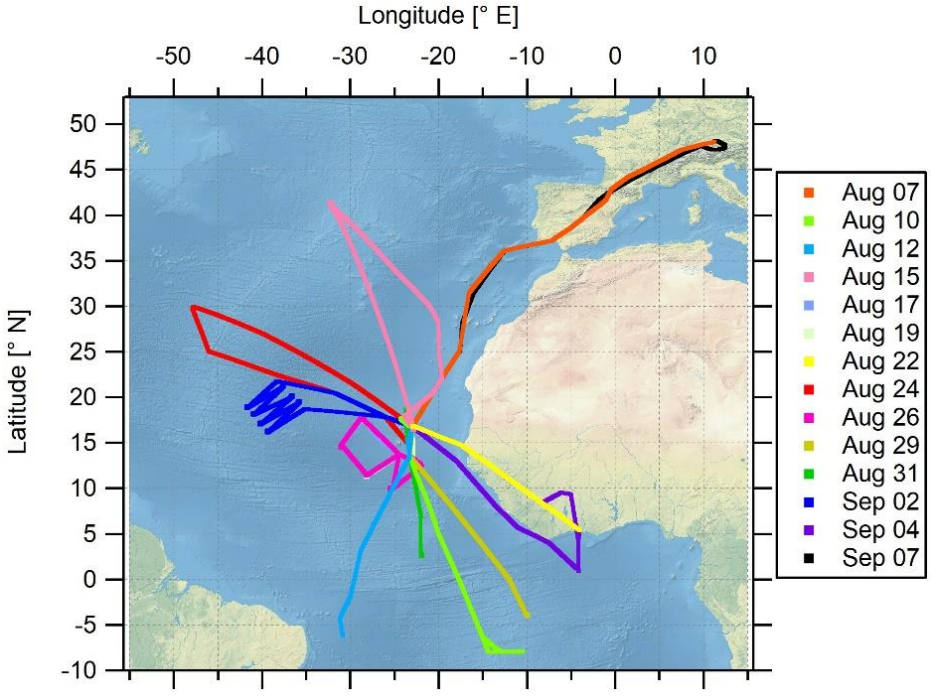

Figure 1: Spatial orientation of the measurement flight tracks during CAFE-Africa. Note that MF07 (August 17, 2018), MF08 (August 19, 2018) and MF11 (August 26, 2018) had identical flight tracks.

Further changes made to the manuscript

We have made the following additional changes to the manuscript, which are not related to the referee's comments and listed below:

Change 1: We have replaced "TDLAS" by "TDL" for the measurement technique/method of H_2O in Table 1 as it is also mentioned as "TDL" in the manuscript.

Change 2: We have added QCLAS **Q**uantum **c**ascade **l**aser **a**bsorption **s**pectroscopy to "Appendix: Acronyms and Abbreviations".

Central role of nitric oxide in ozone production in the upper tropical troposphere over the Atlantic Ocean and West Africa

Ivan Tadic[1], Clara M. Nussbaumer[1], Birger Bohn[2], Hartwig Harder[1], Daniel Marno[1], Monica Martinez[1], Florian Obersteiner[3], Uwe Parchatka[1], Andrea Pozzer[1,4], Roland Rohloff[1], Martin Zöger[5], Jos Lelieveld[1,6] and Horst Fischer[1]

[1]Atmospheric Chemistry Department, Max Planck Institute for Chemistry, Mainz, Germany
[2]Institute of Energy and Climate Research, IEK-8: Troposphere, Forschungszentrum Jülich GmbH, Jülich, Germany
[3]Karlsruhe Institute of Technology, Karlsruhe, Germany
[4]Earth System Physics section, The Abdus Salam International Centre for Theoretical Physics, Trieste, Italy
[5]Flight Experiments, German Aerospace Center (DLR), Oberpfaffenhofen, Germany
[6]Climate and Atmosphere Research Center, The Cyprus Institute, Nicosia, Cyprus

Correspondence: Ivan Tadic (i.tadic@mpic.de) or Horst Fischer (horst.fischer@mpic.de)

Abstract. Mechanisms of tropospheric ozone (O_3) formation are generally well understood. However, studies reporting on net ozone production rates (NOPRs) directly derived from in situ observations are challenging, and are sparse in number. To analyze the role of nitric oxide (NO) in net ozone production in the upper tropical troposphere above the Atlantic Ocean and the West African continent, we present in situ trace gas observations obtained during the CAFE-Africa (**C**hemistry of the **A**tmosphere: **F**ield **E**xperiment in **Africa**) campaign in August and September 2018. The vertical profile of in situ measured NO along the flight tracks reveals lowest NO mixing ratios of less than 20 pptv between 2 and 8 km altitude and highest mixing ratios of 0.15-0.2 ppbv above 12 km altitude. Spatial distribution of tropospheric NO above 12 km altitude shows that the sporadically enhanced local mixing ratios (> 0.4 ppbv) occur over the West African continent, which we attribute to episodic lightning events. Measured O_3 shows little variability in mixing ratios at 60-70 ppbv, with slightly decreasing and increasing tendencies towards the boundary layer and stratosphere, respectively. Concurrent measurements of CO, CH_4, OH and HO_2 and H_2O enable calculations of NOPRs along the flight tracks and reveal net ozone destruction at -0.6 to -0.2 ppbv h^{-1} below 6 km altitude and balance of production and destruction around 7-8 km altitude. We report vertical average NOPRs of 0.2-0.4 ppbv h^{-1} above 12 km altitude with NOPRs occasionally larger than 0.5 ppbv h^{-1} over West Africa coincident with enhanced NO. We compare the observational results to simulated data retrieved from the general circulation ECHAM/MESSy Atmospheric Chemistry (EMAC) model. Although the comparison of mean vertical profiles of NO and O_3 indicates good agreement, local deviations between measured and modelled NO are substantial. The vertical tendencies in NOPRs calculated from simulated data largely reproduce those from in situ experimental data. However, the simulation results do not agree well with NOPRs over the West African continent. Both measurements and simulations indicate that ozone formation in the upper tropical troposphere is NO_x-limited.

1 Introduction

The importance of nitrogen oxides (NO_x = NO + NO_2) and ozone (O_3) in the photochemistry of the atmosphere is widely acknowledged. Both NO and NO_2 are toxic gases, which degrade surface air quality and regulate the abundance of secondary tropospheric oxidants (Hosaynali Beygi et al., 2011; Silvern et al., 2018). They are the propagating agents in the formation of O_3 and govern photochemical ozone production and removal from the atmosphere (Bozem et al., 2017; Schroeder et al., 2017). Ozone is a greenhouse gas, negatively affects human health and causes ecosystem damage (Jaffe et al., 2018). It is the primary precursor of the hydroxyl (OH) radical, which determines the oxidation capacity of the atmosphere and directly controls the concentrations of methane (CH_4), carbon monoxide (CO) and many volatile organic compounds (VOCs) (Thornton et al., 2002; Bozem et al., 2017). The U.S. Clean Air Act identified ozone as a criteria air pollutant in the 1970s (Jaffe et al., 2018). Since then and especially in the last decades, increasing effort has been put in the understanding and mitigation of tropospheric ozone pollution (Fiore et al., 2002; Dentener et al., 2005; West and Fiore, 2005; Lelieveld et al., 2009, Pusede et al., 2015; Jaffe et al., 2018; Nussbaumer and Cohen, 2020; Tadic et al., 2020). To further resolve the complexity of scientific and policy-related issues of the NO_x-O_3-VOCs relationship, careful evaluation of model simulations against in situ measurement data is required (Sillman et al., 1995).

Photochemical ozone formation in the troposphere has been comprehensively described in the literature. Briefly, O_3 is photochemically formed in chemical reactions between NO_x, HO_x (= OH + HO_2) and VOCs (Crutzen, 1974, Schroeder et al., 2017). VOCs are here referred to as RH where R stands for an organic residual. The oxidation of CO, CH_4 and VOCs by OH results in the production of HO_2 and peroxy radicals (RO_2).

$$OH + CO + O_2 \rightarrow HO_2 + CO_2 \quad \text{(R1)}$$

$$OH + CH_4 + O_2 \rightarrow CH_3O_2 + H_2O \quad \text{(R2)}$$

$$OH + RH + O_2 \rightarrow RO_2 + H_2O \quad \text{(R3)}$$

HO_2 and RO_2 (including CH_3O_2 and further organic peroxy radicals) rapidly oxidize NO to NO_2, which will yield O_3 in its subsequent photolysis (reaction R6) followed by recombination of atomic ground-state oxygen with molecular oxygen (reaction R7) (Thornton et al., 2002).

$$NO + HO_2 \rightarrow NO_2 + OH \quad \text{(R4)}$$

$$NO + RO_2 \rightarrow NO_2 + RO \quad \text{(R5)}$$

$$NO_2 + h\nu \rightarrow NO + O(^3P) \quad \text{(R6)}$$

$$O(^3P) + O_2 + M \rightarrow O_3 + M \quad \text{(R7)}$$

The net effect of reaction R1-R7 on HO_x and NO_x is zero, which is why both act as catalysts in photochemical O_3 production. Ozone loss is due to photolysis (and subsequent reaction of $O(^1D)$ with H_2O) and reactions of O_3 with OH and HO_2.

$$O_3 + h\nu \rightarrow O(^1D) + O_2 \quad \text{(R8)}$$

$$O(^1D) + H_2O \rightarrow 2OH \quad \text{(R9)}$$

$$O_3 + OH \rightarrow HO_2 + O_2 \quad \text{(R10)}$$

$$O_3 + HO_2 \rightarrow OH + 2O_2 \quad \text{(R11)}$$

Note that the deactivation of $O(^1D)$ to $O(^3P)$ via collisions with N_2 and O_2 will result in the reformation of O_3 (Bozem et al., 2017; Tadic et al., 2020). We express the portion of O_3 that is effectively lost via photolysis by α (see section 2.2). In this study, we neglect chemical loss reactions of O_3 with alkenes, sulphides and halogen radicals. Note that reactions R8-R11 will be referred to as gross ozone loss, while the rate-limiting reactions of NO with HO_2 or RO_2 to produce NO_2 will be referred to as gross ozone production (Zanis et al., 2000a; Thornton et al., 2002). The difference between these two quantities will yield net ozone production, conventionally given in units of ppbv h^{-1} (Bozem et al., 2017) or ppbv d^{-1} (Tadic et al., 2020).

The dependency of NOPRs on ambient levels of NO_x is highly non-linear (Bozem et al., 2017). Due to the above-mentioned chemistry gross ozone loss will naturally prevail over gross ozone production at low NO_x. Increasing ambient NO_x will result in a linear increase in ozone formation such that the chemical air mass will shift from net destruction to net production in ozone (Bozem et al., 2017; Schroeder et al., 2017). However, at a certain NO mixing ratio, which depends on ambient levels of HO_x and VOCs, adding more NO to the system will result in a saturation in ozone formation and eventually in a decrease in net ozone production towards higher NO levels (Tadic et al., 2020). This is due to the reaction of NO_2 with OH to produce HNO_3 followed by its deposition to the surface.

$$NO_2 + OH + M \rightarrow HNO_3 + M \quad \text{(R12)}$$

Reaction R12 will decrease the pool of available HO_x and NO_x radicals from the atmosphere to produce O_3 (Thornton et al., 2002). Ozone formation hence crucially depends on whether NO_x or VOCs are available in excess. These two atmospheric states are commonly referred to as either VOC-limited (if NO_x is available in excess) or as NO_x-limited (if VOCs are available in excess) (Sillman et al., 1995; Sillman et al., 2003; Duncan et al., 2010; Nussbaumer and Cohen, 2020; Tadic et al., 2020).

The lifetime of NO_x in the atmosphere varies from a few hours in the planetary boundary layer (PBL) to 1-2 weeks in the upper troposphere/lower stratosphere (UTLS) (Beirle et al., 2010). In the latter, the reaction of NO_2 with OH during daytime and NO_3 formation at nighttime is slowed down due to low ambient pressure and temperature. Transport of NO_x from polluted regions to pristine areas is limited due to the short lifetime of NO_x in the PBL (Reed et al., 2016), which is why NO_x in the troposphere can vary over several orders of magnitude (Miyazaki et al., 2017; Tadic et al., 2020). Whilst measurements performed in remote and pristine regions, such as in the unpolluted South Atlantic marine boundary layer (MBL), have reported NO_x mixing ratios of only a few tens of pptv (Hosaynali Beygi et al., 2011; Fischer et al., 2015), NO_x mixing ratios in urban areas can exceed several tens of ppbv (Lu et al., 2010). Measurements obtained in the polluted MBL around the Arabian Peninsula have shown that NO_x mixing ratios can locally exceed several tens of ppbv even in marine environments in the proximity to strong emission sources such as passing ships or downwind of megacities (Tadic et al., 2020).

Ground-level NO_x emissions include fossil fuel combustion, biomass burning and soil emissions (Silvern et al., 2018). Lightning NO_x (LNO_x), aircraft emissions, and, to a lesser extent, convective uplift of potentially NO_x-rich planetary boundary air and intrusion of stratospheric air are predominant sources of NO_x in the upper troposphere (Bozem et al., 2017; Miyazaki et al., 2017). However, estimates of lightning produced NO_x are uncertain (Beirle et al., 2010; Miyazaki et al., 2017) and can have large implications on the photochemistry of the upper troposphere such as over tropical areas where lightning flash rates are enhanced (Christian et al., 2003; Tost et al. 2007).

A number of previous studies have performed measurements in the region of interest, the troposphere over the Atlantic Ocean and the West Africa (Lelieveld et al., 2004; Aghedo et al., 2007; Saunois et al., 2009; Real et al., 2010; Bourgeois et al., 2020). Lelieveld et al. (2004) indicated that positive ozone trends in the marine boundary layer over the Atlantic are likely caused by an increase in anthropogenic emissions of nitrogen oxides. Aghedo et al. (2007) showed that lightning acts as a major source of tropospheric NO_x, leading to a significant increase in middle and upper tropospheric ozone over the African continent. Saunois et al. (2009) described results from airborne measurements in the region during the AMMA project. Deploying a two-dimensional model for further analysis, Saunois et al. determined positive trends in photochemical net ozone production in the boundary layer over West Africa. There are also results from the ATom airborne mission, which measured vertical profiles of O_3 in the troposphere over the Atlantic Ocean (Bourgeois et al., 2020), which we will use to validate the results presented here. Real et al. (2010) investigated downwind O_3 production in pollution plumes in the mid and upper troposphere and determined mean net ozone production rates of 2.6 ppbv/day over a period of 10 days. However, studies reporting on vertical profiles and spatial distributions of nitric oxide, ozone and net ozone production rates as part of one coherent measurement project in the troposphere over the West African continent and the Atlantic Ocean are absent.

In the present study, we characterize the distribution of NO and the role of NO in photochemical processes in the upper tropical troposphere above the Atlantic Ocean and West Africa. The structure of the paper is as follows: we provide methodological, practical and technical information about the campaign and deployed instrumentation in Sect. 2. In Sect. 3 we present in situ NO and O_3 data obtained during the campaign including vertical profiles and spatial distributions. Based on concurrent measurements of CO, CH_4, OH and HO_2, H_2O, the actinic flux density, pressure and temperature net O_3 production rates (NOPRs) were calculated along the flight tracks. We also provide a comparison of the observational results to simulated data retrieved from the 3-D EMAC model and analyze the dependency of NOPRs on ambient NO. In Sect. 4, we summarize our results and draw conclusions based on our findings.

2 Experimental

2.1 CAFE-Africa campaign

The airborne measurement-based CAFE-Africa project took place in August and September 2018 in the tropical troposphere over the Central Atlantic Ocean and the West African continent. Starting from and returning to the international airport on Sal, Cape Verde (16.75° N, 22.95° W) a total of 14 scientific measurement flights (MFs) was carried out with the German **H**igh

Altitude and **Lo**ng-range research aircraft (HALO). For the analysis of the MFs, we consecutively numerate each MF, starting with MF03 on August 07, 2018 for the ferry flight from Oberpfaffenhofen (Germany, Deutsches Zentrum für Luft- und Raumfahrt) to Sal (Cape Verde Islands) on and ending with MF16 on September 07, 2018 for the back ferry flight from Sal to Oberpfaffenhofen on. The test flights MF01 and MF02 conducted over Germany are not included in this study. MF03-MF16 covered a latitudinal range from 8° S to 48.2° N and a longitudinal range from 47.9° W to 12.5° E and reached maximum flight altitudes of about 15 km. Before landing at the home base airport in Sal, a fixed-altitude leg of 30 min duration at FL150 (~4,600 m altitude) was flown for calibration purposes. Take off (T/O) time of the flights was typically 9 or 10 UTC, except for MF08 with T/O at 4 UTC and landing around 13 UTC and MF11 with T/O at 16 UTC and landing around 1 UTC the next day.

The location of the campaign home base on Sal provided the unique possibility to analyze the impact of the **I**nter-**T**ropical **c**onvergence **z**one (ITCZ) on physical and chemical processes in the airspace above the Atlantic Ocean and the West African continent. The ITCZ is a low-pressure region evolving near the equator, which is characterized by deep convection, strong precipitation and frequent lightning (Collier and Hughes, 2011), producing nitrogen oxides, mostly as NO through the Zeldovich reactions from atmospheric N_2 and O_2. The campaign was performed in late summer (August and September) 2018 when the ITCZ had reached its northernmost position at around 5-15° N (Collier and Hughes, 2011) and was henceforth located only a few degrees in latitude to the south of the campaign base at 16.75° N. The flight tracks of the 14 MFs performed during the campaign are shown in Fig. 1. An overview of the corresponding flight dates and objectives of each particular MF is given in the supplementary Table ST1.

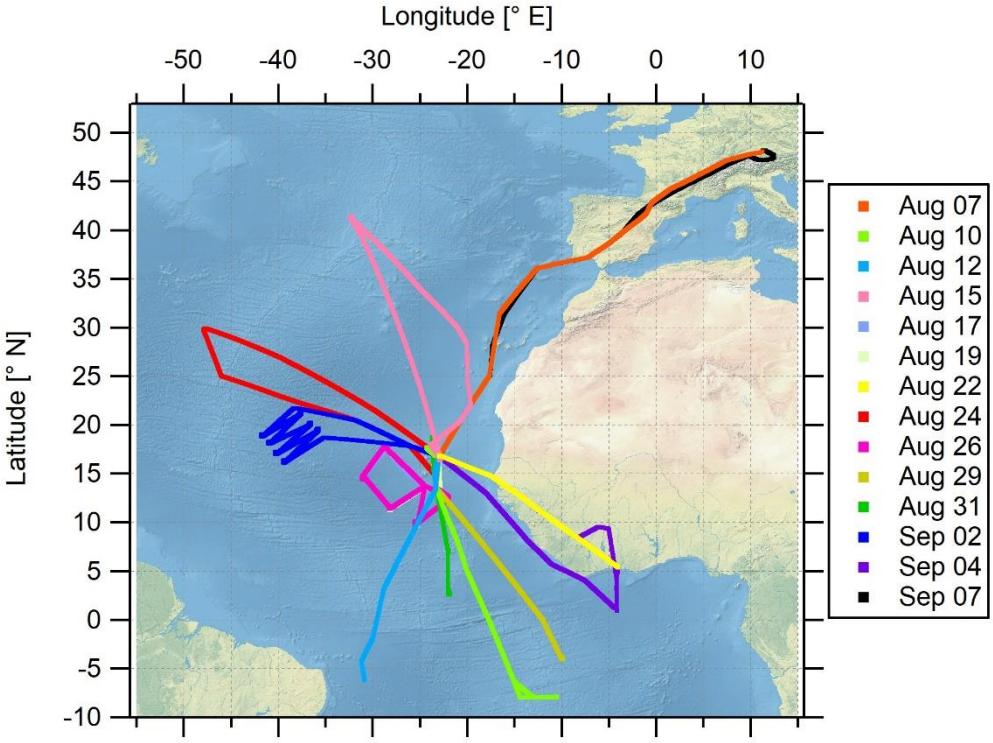

Figure 1: Spatial orientation of the measurement flight tracks of during CAFE-Africa. Note that MF07 (August 17, 2018), MF08 (August 19, 2018) and MF11 (August 26, 2018) had identical flight tracks.

2.2 Chemiluminescent detection of NO

In situ measurements of NO_x on ground-based and mobile platforms are challenging in terms of the demand for high sensitivity and high precision (Tadic et al., 2020). During CAFE-Africa, we deployed a modified commercially available chemiluminescent detector *CLD 790 SR* (ECO Physics Inc., Dürnten, Switzerland) on-board HALO. It is the same instrument that has been used during previous shipborne (Hosaynali Beygi et al., 2011; Tadic et al., 2020) and airborne campaigns (Bozem et al., 2017). The measurement method is based on the gas phase reaction of NO with O_3, which will partly produce excited-state NO_2^* followed by the spontaneous emission (chemiluminescence) of a photon (Ridley and Howlett, 1967; Ryerson et al., 2000).

$$NO + O_3 \rightarrow NO_2^* + O_2 \quad \text{(R13)}$$

$$NO_2^* \rightarrow NO_2 + h\nu \ (\lambda > 600 \text{ nm}) \quad \text{(R14)}$$

Photons generated through the emissions from excited-state NO_2^*, which are directly proportional to the NO concentration in the sample flow (Ridley and Howlett, 1967), are detected by a photomultiplier tube and converted to an electric pulse. Carrying out the oxidation of NO by O_3 at low-pressure (7-8 mbar) and in a temperature-stabilized (25 °C) main reaction chamber,

minimizes quenching (non-radiative de-excitation of NO_2^* via collisions) (Reed et al., 2016; Tadic et al., 2020). Detector dark noise and artefacts due to the reaction of O_3 with species other than NO (such as alkenes and sulphides) is corrected for by using a pre-chamber setup, as first described by Ridley and Howlett (1967). A residual instrumental background (due to memory effects within the instrument) is corrected for by regularly sampling synthetic zero air (Tadic et al., 2020). During the MFs, we sampled zero air from a tank (17 l composite tank, AVOX) with a Purafil-activated carbon adsorbent installed downstream of the zero-air tank to ensure NO-free zero-air measurements. The residual instrumental background of the NO measurement was calculated at 5 pptv from measurements obtained at nighttime during MF11. As chemiluminescent detection of NO is an indirect measurement method, regular calibrations against a known standard are needed. During the MFs we diluted the secondary NO standard (1.187 ± 0.036 ppmv NO in N_2) at a mass flow of 8.6 sccm in a zero-air flow of 3.44 SLM (standard litre per minute) resulting in NO calibration gas mixing ratios of ~3 ppbv. NO calibrations measurements were performed six to eight times during a MF of 9-10 h duration by manually initiating calibration slots consisting of 2 min zero-air measurement, 2 min NO calibration and 2 min zero-air measurement, similar to previous deployments of the instrument (see Tadic et al., 2020).

The limit of detection (LOD) of the NO data was calculated at 9 pptv from the FWHM (full width at half maximum) of a Gauss Fit applied to the distribution of 1 s NO data obtained at nighttime during MF11 (see supplement Figure S1). Analogously we estimate the LOD of the NO data at 1 min time resolution to be 5 pptv from the FWHM of a Gauss Fit applied to the distribution of 1 min NO data obtained at nighttime during MF11. The precision of the NO data was calculated from the average reproducibility of all in-flight calibrations to be 5 % at 1σ. The uncertainty in the used secondary standard mixing ratio was 3 %. The total measurement uncertainty (TMU) of the NO data was estimated at 6 % as the quadratic sum of the precision and the uncertainty of the secondary standard (Tadic et al., 2020).

$$\mathrm{TMU(NO)} = \sqrt{(5\,\%)^2 + (3\,\%)^2} \approx 6\,\% \quad (1)$$

2.3 Further measurements used in this study

O_3 was quantified with a chemiluminescence detector calibrated by a UV photometer (**F**ast **AIR**borne **O**zone Instrument; Zahn et al., 2012). CO and CH_4 were measured by mid-infrared quantum cascade laser absorption spectroscopy (QCLAS) with TRISTAR, a multi-channel spectrometer (Schiller et al., 2008; Tadic et al., 2017). OH and HO_2 radicals were measured by laser-induced fluorescence with the custom-built HORUS instrument (Marno et al., 2020). Note that both OH and HO_2 data are preliminary. We conservatively estimate the total relative measurement uncertainty of the OH and HO_2 data at 50 %. Spectrally resolved actinic flux density measurements were obtained with two spectro-radiometers (upward- and downward-looking) installed on the top and bottom of the aircraft fuselage, respectively. The particular photolysis frequencies were calculated from the actinic flux density spectra between 280 and 650 nm (Bohn and Lohse, 2017). The uncertainty in the used *j*-values was estimated to be 13 %. Water vapor mixing ratio and further derived humidity parameters were measured by SHARC (**S**ophisticated **H**ygrometer for **A**tmospheric **R**esear**C**h) based on dual path direct absorption measurement by a

tunable diode laser (TDL) system (Krautstrunk and Giez, 2012). The measurement range of SHARC covers the whole troposphere and lower stratosphere (5-40000 ppmv) with an absolute accuracy of 5 % (+1 ppmv). The BAMAHAS (**BA**sic **HA**LO **M**easurement **A**nd **S**ensor System) provided measurements of temperature and pressure (Krautstrunk and Giez, 2012). All instruments deployed on the aircraft have been developed to meet the high standards of airborne measurements in terms of operability, accuracy and sensitivity. Table 1 lists the used instrumentation with the associated total measurement uncertainties. A reference is given regarding the use of each method during previous measurements.

Table 1: List of performed observations with the corresponding total measurement uncertainty (given as a percentage) during CAFE-Africa. The last column provides a reference regarding the practical use of the used measurement/instrument.

Measurement	Technique / method	TMU	reference
NO	chemiluminescence	6 %	Tadic et al., 2020
O_3	UV photometry / chemiluminescence	2.5 %	Zahn et al., 2012
CO	QCLAS	4.3 %	Tadic et al., 2017
CH_4	QCLAS	0.3 %	Schiller et al., 2008
OH	LIF	50 %	Marno et al., 2020
HO_2	LIF with chemical conversion	50 %	Marno et al., 2020
H_2O	TDL	5 %	Krautstrunk and Giez, 2012
$j(O^1D)$	spectral radiometer	13 %	Bohn and Lohse, 2017

2.4 ECHAM/MESSy Atmospheric Chemistry (EMAC) model and data analysis

EMAC is a 3-D global general circulation, atmospheric chemistry-climate model, which has been used and described in a number of previous studies (Roeckner et al., 2006; Jöckel et al., 2010; Sander et al., 2019; Tadic et al., 2020). Briefly, EMAC comprises the 5th generation of the **E**uropean **C**enter **Ham**burg (ECHAM5) circulation model (Roeckner et al., 2006) and the **M**odular **E**arth **S**ubmodel **Sy**stem (MESSy) in the version 2.52 (Jöckel et al., 2010). Here we use the model in the T63L47 resolution with a spatial resolution of roughly 1.8° × 1.8°, 47 vertical levels and one data point every 6 min. The model has been weakly nudged towards the ECMWF ERA-Interim data (Jeucke et al., 1996; Berrisford et al., 2009). The chemical mechanism (the Mainz Organic Mechanism, MOM) and the photolysis rate calculations used in this work have been presented in Sander et al. (2019) and in Sander et al. (2014), respectively. The Emissions Database for Global Atmospheric Research (EDGARv4.3.2, Crippa et al. 2018) were used for anthropogenic emissions, while biomass burning emissions were from the GFAS (Global Fire Assimilation System) database with a daily temporal resolution (Kaiser et al 2012). Important for this work, the NO_x emissions from lightning activity have been estimated using the submodel LNOX (Tost et al., 2007), where the parameterization by Grewe et al. (2001) was applied. The global NO_x emissions from lightning were scaled to 6.3 Tg(N)/yr, following Miyazaki et al. (2014). Tracer and aerosol wet and dry deposition were estimated following Tost et al. (2006) and Kerkweg et al. (2006), respectively. The NO_x soil biogenic emission flux is calculated based on a semi-empirical emission algorithm implementation by Yienger and Levy II (1995; Kerkweg et al., 2006). For the current study we use EMAC simulations of NO, O_3, OH, HO_2, CH_3O_2, specific humidity, $j(O^1D)$, temperature and pressure spatially interpolated to the flight tracks (latitude, longitude and altitude). Based on the simulations we perform calculations of α and NOPRs along the

flight tracks (see section 2.5). To synchronize the time stamp of the model data (6 min) with the measurement data (1 min), we have calculated a running mean of the measurement data within ±2 min around the simulated data point along the measurement flight tracks such that every sixth measurement data point (if available) was neglected.

2.5 Calculation of net ozone production rates (NOPRs)

Calculation of NOPRs utilizes the chemical reactions related to ozone formation described in the introduction. EMAC model calculations show that during CAFE-Africa CH_3O_2 represents on average 80 % of the sum of all organic peroxy radicals with respect to ozone formation at typical flight altitudes of 200 hPa (and even up to 90 % at lower altitudes). Model calculations further show that the sum of HO_2 and CH_3O_2 represents on average 95 % of the sum of HO_2 and all organic peroxy radicals (RO_2) yielding that the ratio $(HO_2+CH_3O_2)/(HO_2+RO_2)$ is practically one. In analogy to Tadic et al. (2017), we estimated RO_2 as the sum of all organic peroxy radicals with less than four carbon atoms. See supplementary Table ST2 for an overview of the used organic peroxy radicals. Therewith we calculate photochemical gross production of O_3 by the rate-limiting reaction of NO with HO_2 and CH_3O_2 (Thornton et al., 2002; Bozem et al., 2017).

$$P(O_3) = [NO] \cdot (k_{NO+HO_2}[HO_2] + k_{NO+CH_3O_2}[CH_3O_2]). \quad (2)$$

The IUPAC Task Group on Atmospheric Chemical Kinetic Data Evaluation (Atkinson et al. 2004; Atkinson et al., 2006) provides rate coefficients used in this study. Note that other studies use $P(O_3)$gross as an acronym for $P(O_3)$ in Eq. 2. The photochemical lifetimes of both HO_2 and CH_3O_2 are similar with respect to self-reactions yielding hydrogen peroxide and methyl hydroperoxide and reactions with NO and HO_x (Bozem et al., 2017). We further assume photostationary steady state (PSS) for the probed air masses. As the typical time to acquire PSS during CAFE-Africa varied between 40 s at 2 km altitude and about 70-80 s at 15 km altitude (Mannschreck et al., 2004; Tadic et al., 2020), we can calculate the concentration of CH_3O_2 by the equation derived by Bozem et al. (2017).

$$[CH_3O_2] = \frac{k_{OH+CH_4}[CH_4]}{k_{OH+CO}[CO]} \cdot [HO_2] \quad (3)$$

Note that the reaction of CO with OH represents the dominant term in HO_2 production during CAFE-Africa. Assuming mixing ratios of 500 ppbv and 100 pptv for H_2 and HCHO, respectively, we find that HO_2 production rate from the reaction of OH with CO is on average 5 times greater than the sum of the HO_2 production rates from photolysis of HCHO and the reactions of HCHO and H_2 with OH during CAFE-Africa. Note that the assumed mixing ratio of 100 pptv represents a rather conservative upper estimate for HCHO in the upper troposphere. As mentioned above, ozone loss due to photolysis (and subsequent reaction of $O(^1D)$ with H_2O) will only partly lead to a net loss effect as most $O(^1D)$ will deactivate via collisions with air molecules, mostly N_2 and O_2, to $O(^3P)$ and reform O_3 in the subsequent reaction with O_2. The share of O_3 photolysis that will eventually lead to a net loss in O_3, can be calculated using Eq. 4 (Bozem et al., 2017; Tadic et al., 2020).

$$\alpha = \frac{k_{O(^1D)+H_2O}[H_2O]}{k_{O(^1D)+H_2O}[H_2O]+k_{O(^1D)+N_2}[N_2]+k_{O(^1D)+O_2}[O_2]} \quad (4)$$

In the troposphere, α ranges from about 15 % in the PBL to 1 % in the upper troposphere, where absolute humidity is very low (Bozem et al., 2017). Further loss processes of O_3 (reactions with alkenes, sulphides and halogen radicals) are considered small and are therefore neglected in this study. Equation 5 then gives gross loss of ozone.

$$L(O_3) = [O_3] \cdot (\alpha \cdot j(O^1D) + k_{OH+O_3}[OH] + k_{HO_2+O_3}[HO_2]) \quad (5)$$

$j(O^1D)$ expresses the photolysis frequency of ozone to $O(^1D)$. The NOPR is given as the difference of the gross ozone production rate (Eq. 2) and the gross ozone loss rate (Eq. 5) (Lin et al., 1988, Cantrell et al., 2003).

$$\text{NOPR} = P(O_3) - L(O_3) =$$

$$[NO] \cdot \left(k_{NO+HO_2}[HO_2] + k_{NO+CH_3O_2}[CH_3O_2]\right) - [O_3] \cdot (\alpha \cdot j(O^1D) + k_{OH+O_3}[OH] + k_{HO_2+O_3}[HO_2]) \quad (6)$$

Note that other studies use $P(O_3)$net as an acronym for NOPR in Eq. 6.

3 Results

3.1 Vertical profiles of NO and O_3 in the tropical troposphere

In the following, we will investigate averages of the vertical profiles, which are calculated based on an altitude bin width of 1 km. The profiles are calculated with respect to the centre of the particular bin, e.g. the average at 3.5 km includes all data points obtained at or above 3 km altitude and below 4 km altitude. Data are filtered for stratospheric influence by removing all data points for which concurrent O_3 is larger than 100 ppbv; a conservative criterion which has been discussed by Prather et al. (2011). Fig. 2 shows the vertical NO and O_3 profiles obtained during CAFE-Africa. The orange and blue lines represent vertical average profiles of experimental and model simulated data, respectively. The blue and orange shading in the respective colors represent the ± 1 standard deviation of the vertical averages.

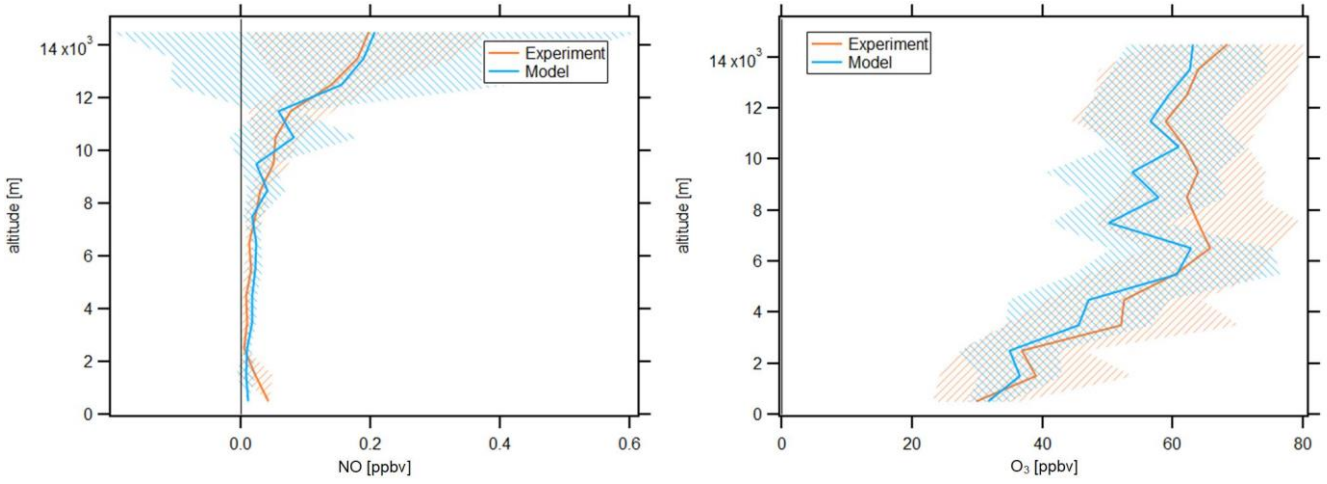

Figure 2: Vertical NO (left) and O_3 profiles (right) of measured and modelled data along the flight tracks during CAFE-Africa. Note the large variability of simulated NO mixing ratios above 10 km. The figures have been filtered for stratospheric measurements by removing data points for which O_3 exceeds 100 ppbv.

The vertical profile of measured NO data shows lowest NO mixing ratios of less than 20 pptv observed between 2 and 8 km altitude, which reflect the absence of emission and transport sources at these altitudes. Highest NO mixing ratios of 0.15-0.2 ppbv are observed above 12 km altitude and reflect the increasing amount of lightning-produced NO_x, and to a lesser extent influence of relatively NO_x-rich stratospheric air. Below 2 km altitude, the vertical profile shows a weak increase of NO, which reproduces the low amount of anthropogenic sources in the investigated MBL and PBL in the proximity to the Cape Verde Islands. This suggests that the contribution of local convective uplift of PBL air to the increased NO_x above 12 km altitude is negligible.

The vertical average profile of simulated NO data is in good agreement with the vertical profile of measured NO data, which is also indicated by the median NO(model)/NO(measurement) ratio throughout the whole campaign at 0.97. Although the vertical profiles are in overall agreement, the variability when comparing single measurement and simulation data points is substantial, as indicated by the large variability of simulated NO data above 10 km altitude. The 25th percentile, 75th percentile and average of the NO(model)/NO(measurement) ratio throughout the whole campaign are 0.25, 2.2 and 2.27, respectively, which illustrate the significant spread among measurement and model data in a comparison of individual data points. The minimum and maximum mixing ratios of modelled NO are zero and 2.13 ppbv, respectively. The minimum and maximum mixing ratios of observed NO are zero and 0.95 ppbv, respectively.

The average vertical profile of measured O_3 shows lowest mixing ratios of 30-40 ppbv below 3 km altitude and a steady increase in O_3 at about 5-10 ppbv per km altitude to mixing ratios of 60-65 ppbv at 6 km. Above this altitude, O_3 is relatively constant (60-65 ppbv) until it further increases above 12 km altitude, simultaneous with the increase in NO.

Although simulated O_3 slightly underestimates the measurement data throughout the troposphere, we find that the vertical profiles of simulated and measured O_3 data are in again in good agreement. EMAC O_3 data match lowest mixing ratios of 30-40 ppbv observed below altitudes of 3 km as well as the vertical gradient in O_3 mixing ratios between 3 and 6 km with mixing ratios of 60 ppbv at 6 km altitude. Above 6 km altitude, both the vertically constant O_3 mixing ratio as well as the further increase in O_3 above 12 km altitude deduced from the measurements are well reproduced by the model. Except for lowest altitudes (< 1 km), it seems that simulated O_3 mixing ratios slightly underestimate the measurement data. This is confirmed by the median and average O_3(model)/O_3(measurement) ratio throughout the campaign at 0.97 and 0.98, respectively, confirming the general agreement between measurements and simulations, as well as the slight underestimation by the latter. The 25th percentile and 75th percentile of the O_3(model)/O_3(measurement) ratio are 0.85 and 1.11, respectively, and indicate that the spread among single data points when comparing measurement and model for O_3 is less than for NO.

O_3 profiles observed in this study are in good agreement with results from the ATom mission (Bourgeois et al., 2020). For the June-August season, Bourgeois et al. show that in the tropical troposphere O_3 increased with altitude to 50 ppbv at 5-6 km whereas above 9 km O_3 varied from 40 to 80 ppbv, supporting the results presented here (see Figures 9 and 10 in Bourgeois et al., 2020).

3.2 Spatial distribution of NO and O_3 in the upper tropical troposphere

As most of the measurement time (> 60 %) of the CAFE-Africa campaign was dedicated to upper tropospheric measurements above 12 km altitude and as both NO and O_3 show highest mean mixing ratios above 12 km altitude, we characterize the spatial distribution of NO and O_3 above that altitude in the following. Data above 12 km altitude have been aggregated and averaged over a spatial 2° × 2° grid. We again remove stratospheric measurement data by only considering those for which O_3 was below 100 ppbv. Note that this does not necessarily exclude influence of mixing with air of stratospheric origin. Figure 3 shows the color-coded spatial NO distributions based on the measured data (left plot) and simulated data (middle plot). The right plot shows the tropospheric average spatial distribution of the point-by-point NO(model)/NO(measurement) ratio above 12 km. Note that the color scales presented in the following emphasize the most relevant features of the spatial distribution. Thus a few single data points might exceed the given color range, such as in the case of simulated NO (Figure 3, middle plot) with single maximum NO mixing ratios of > 1 ppbv.

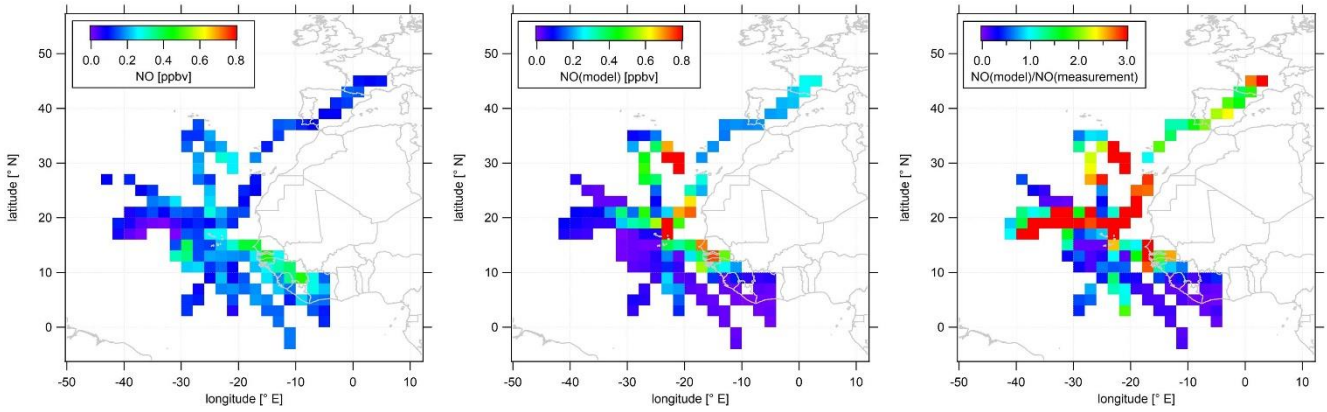

Figure 3: Color-coded spatial, tropospheric NO distributions above 12 km during CAFE-Africa. The left and middle graphs show the measured and simulated NO, respectively. The right graph shows the spatial distribution of the NO(model)/NO(measurement) ratio. The figures have been filtered for stratospheric measurements by removing data points for which O_3 exceeds 100 ppbv.

The spatial distribution of NO from the measurement data shows that NO in the upper tropical troposphere above West Africa and the Atlantic Ocean is generally 0.1-0.2 ppbv. The range in mixing ratios includes lowest NO of less than 20 pptv observed between –30 to –40° E and 16 to 20° N close to a deep convective system without lightning to mixing ratios of 0.1-0.2 ppbv over wide areas over the Atlantic Ocean to (more than) 0.4 ppbv over the West African continent. Although deep convective systems over oceanic regions rarely evolve lightning (Zipser, 1994), we encountered large amounts of NO close to a marine cumulonimbus cloud system with potential lightning activity resulting in more than 0.3 ppbv NO at –28 to –32° E and at 12 to 16° N. The coincidence of the ITCZ (5 to 15° N during August and September) and enhancements in upper tropospheric NO above West Africa underlines the substantial influence of the seasonal migration of the ITCZ and its impact on lightning and nitrogen oxides in the upper tropical troposphere (Zipser, 1994; Xu and Zipser, 2012). The data also suggest a longitudinal increase in NO from about 0.1 ppbv observed at –40° E westbound to 0.4 ppbv above the West African continent. Note that we observe a slight decrease in upper tropospheric NO over the Ivory Coast and partly also over Guinea compared to upper

tropospheric NO over Senegal, although the lightning flash rate over the Ivory Coast and Guinea is reported to be a factor of about 3 larger than that over Senegal (Collier and Hughes, 2011). A linear fit applied to the longitudinal average profile of all NO data weighted by the standard deviation and collected in the troposphere above 12 km altitude between –42° E and –8° E reveals an increase in average NO of 4-5 pptv per degree longitude (see supplement Figure S2).

Although the comparison of the vertical profiles of measured and simulated NO suggests generally good correspondence between measurements and model simulations, the agreement with respect to the spatial NO distributions in the upper troposphere is much less satisfactory. The EMAC model does not reproduce the large NO enhancements in the area of the ITCZ, as shown in the latitudinal profile of measured and simulated tropospheric NO data above 12 km in Figure S3 in the supplement. On contrary the model tends to underestimate the observations south of 10° N. Interestingly, this holds also for observations above the West African continent (except for the airspace over Senegal around 12 to 14° N) where simulated NO mixing ratios are highest. This general underestimation of the measurements by the model over large parts of West Africa extends to large parts of the Atlantic Ocean between 5 to 15° N. On the other hand, further north the model tends to overestimate the measurements across large areas north of 16° N and west of –20° E with spatially averaged mixing ratios that exceed 1 ppbv. However, reasonable agreement between measurements and numerical results is observed towards and over Southern Europe.

Figure 4 shows color-coded spatial O_3 distributions based on observations (left plot) and simulated data (middle plot). The right plot of Figure 4 shows the average tropospheric distribution of the point-by-point O_3(model)/O_3(measurement) ratio. In analogy to supplement Figure S3, supplement Figure S4 shows latitudinal profiles of measured and simulated O_3 mixing ratios obtained above 12 km in the troposphere.

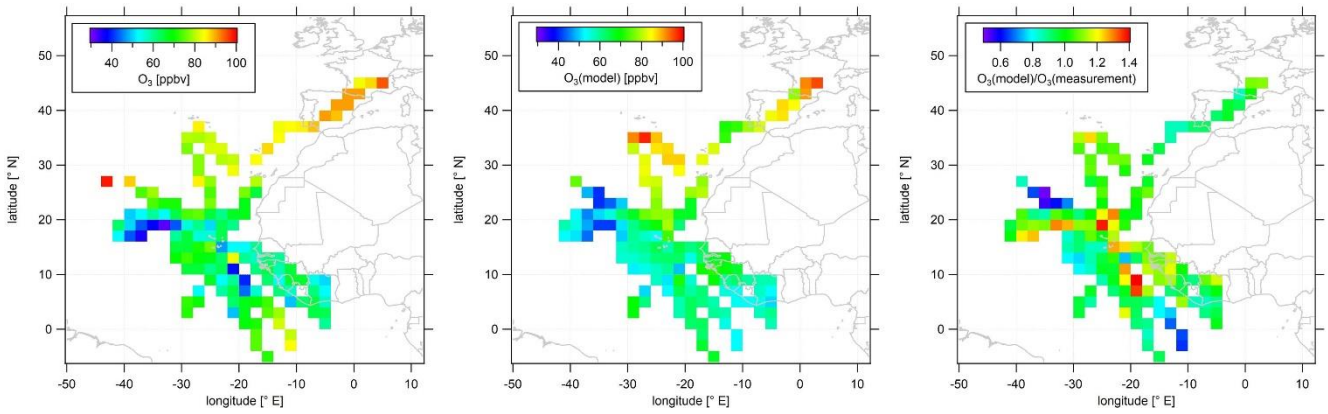

Figure 4: Color-coded spatial, tropospheric O_3 distributions above 12 km during CAFE-Africa. The left and middle graphs show the spatial distribution of measured and simulated O_3, respectively. The right graph shows the spatial distribution of the O_3(model)/O_3(measurement) ratio. The figures have been filtered for stratospheric measurements by removing data points for which O_3 exceeds 100 ppbv.

Measured O_3 shows a rather uniform distribution in the upper troposphere above the Atlantic Ocean and West African continent. The observed mixing ratios range from less than 40 ppbv between –30 to –40° E and 16 to 20° N, areas where NO is likewise decreased, compared to other regions with more than 80 ppbv towards and over Southern Europe, which partly reflects the increasing stratospheric impact above 12 km altitude. Over the West African continent, we observed average O_3 at 50-70 ppbv, which is in approximate agreement with previous studies (Galanter et al., 2000). Note that measured O_3 mixing ratios over the African continent are not significantly different from O_3 mixing ratios over adjacent oceanic areas.

In general, the simulated O_3 reproduces the observed absolute O_3 mixing ratios in the upper tropical troposphere, as well as regional tendencies. It is of note that, although the model underestimates NO over the tropical continental area of Africa, O_3 is reproduced remarkably well. Nevertheless, the model is not able to reproduce local O_3 variations such as at -20° E and 10° N or at -10° E and 0° N. Moreover, simulated O_3 seems to be rather uniformly distributed throughout the whole ITCZ region. The right panel of Figure 4 further illustrates that the majority of the simulated data points deviate by less than 10-15 % from the observational data and that larger deviations between model simulations and measurement are mainly restricted to situations when the measurements show either the lowest or highest mixing ratios, not reproduced by the simulations. The overall spatial agreement between O_3 observation and O_3 simulation is also demonstrated in the latitudinal profile given in supplement Figure S4. Furthermore, supplementary Figures S5 and S6 show 2-D latitudinal/altitudinal distributions of measured, tropospheric NO and O_3, respectively.

3.3 Net ozone production rates in the tropical troposphere

In the following, NOPRs are calculated based on Eq. 6 and analyzed both vertically and spatially. The left graph of Figure 5 shows the vertical profile of NOPRs derived from measured and simulated data in orange and blue ($\pm$1 standard deviation of the corresponding vertical average), respectively. The middle and right graph show the vertical average profiles of the components of gross ozone loss and gross ozone production derived from experimental in situ data and simulated data, respectively. We provide a vertical profile of α calculated based on Eq. 4, for which we obtain good agreement between measurements and simulations, for which we refer to the left graph of Figure S7 in the supplement. Supplementary Figure S7 also provides a comparison of vertical profiles of measured and simulated H_2O mixing ratios. The vertical profiles are calculated based on an altitudinal bin width of 1 km and are filtered for stratospheric influence by removing data points for which O_3 is higher than 100 ppbv. Supplement Figure S8 presents latitudinal profiles of NOPRs above 12 km altitude in the troposphere derived from measured and simulated data. A spatial distribution of OH and HO_2 (derived from both measured and simulated data) is given in the supplement Figure S9.

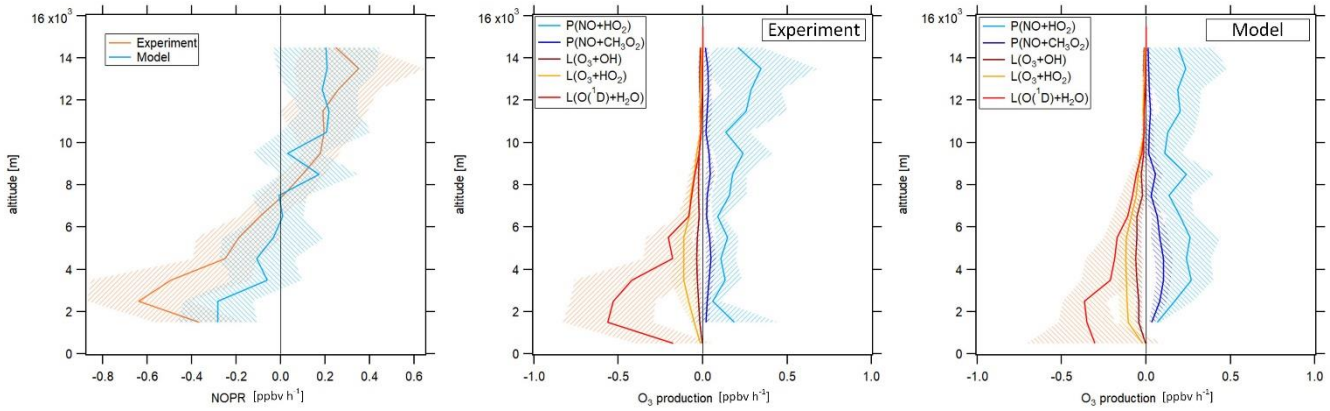

Figure 5: Vertical profile of tropospheric NOPRs calculated based on Eq. 6 during CAFE-Africa (left graph). The orange and blue lines represent NOPR calculations based on measured and simulated data, respectively. The middle and right graphs show the components of net ozone production in Eq. 6 derived from experimental data (middle graph) and simulated data (right graph). The figures have been filtered for stratospheric measurements by removing data points for which O_3 exceeds 100 ppbv

During CAFE-Africa NOPRs derived from in situ measurements varied between -1 ppbv h^{-1} to about 0.6 ppbv h^{-1} within $\pm$ 1 standard deviation of the vertical average. We found net ozone destruction for all altitudes below 7-8 km with a minimum of (-0.6 ± 0.2) ppbv h^{-1} between 2 and 3 km. A general increase of NOPRs with altitude results in net ozone production of 0.2-0.4 ppbv h^{-1} above 9 km altitude with a maximum of (0.4 ± 0.3) ppbv h^{-1} between 13 and 14 km altitude. The large standard deviation associated with the vertical profile at 13-14 km altitude reflects the large variation in NOPRs along the flight tracks. The vertical NOPR profile derived from in situ data further shows a rather smooth transition from net ozone destruction to net ozone production between 7-8 km altitude, which is in good agreement with the value estimated by Bozem et al. (2017) for the tropical troposphere over the South American rainforest at latitudes of 5 to 10° N. The negative net ozone tendencies observed between 3 and 5 km altitude for the tropical troposphere stand in opposition to positive net ozone tendencies of about 0.1 ppbv h^{-1} (Zanis et al., 2000a) and balance in net ozone tendencies (NOPR = 0) (HOOVER campaign over Europe; Bozem et al., 2017) deduced from previous measurements at similar altitudes at mid-latitudes.

In general, the vertical tendencies in NOPRs derived from the observations are well reproduced by the NOPR calculation based on simulated data. However, the model calculations indicate a minimum in net ozone destruction at (-0.3 ± 0.2) ppbv h^{-1} between 1 to 3 km, which represents about half of that derived from the in situ measurements for these altitudes. This underestimation of the measurement by the model is directly related to an underestimation of simulated humidity and $j(O^1D)$, which are both underestimated by EMAC by about 15-20 % below 4 km altitude (see the right graph of supplement Figure S7 for a comparison of the vertical profiles of measured and simulated $j(O^1D)$). The model reports net ozone production of 0.2 ppbv h^{-1} above 8 km (except between 9 and 10 km altitude) and also suggests that the transition from net destruction to net production occurs between 6 and 8 km altitude, which again agrees with the measurement-based calculation. Nevertheless, the atmospheric variability of the (simulation-based) average NOPR profile reveals that transition from net ozone destruction to net ozone production occurs within a wider altitudinal range of 4 to 10 km altitude.

The reaction of NO with HO_2 dominates gross ozone production (middle graphic, Figure 5) for NOPRs derived from measured in situ data. Whilst the reaction of NO with CH_3O_2 contributes about 0.03 ppbv h^{-1} to gross ozone production throughout the whole troposphere, the vertical average of the ozone production rate from the reaction of NO with HO_2 yields 0.1 ppbv h^{-1} at the lowest altitudes with a linear increase ($r^2 \approx 0.6$) to about 0.3 ppbv h^{-1} at 14-15 km altitude. From our observations it follows that the ozone production rate due to the reaction of NO with HO_2 is from a factor of 2-3 (below 3 km altitude) to a factor of 10 (above 12 km altitude) stronger than gross ozone production due to the reaction of NO with CH_3O_2. For the measurement-based estimate, photolysis of ozone dominates gross ozone loss below 6 km altitude. Between 1 and 2 km, it is largest in absolute values at -0.8 ppbv h^{-1}, where it contributes to about 80 % of total gross ozone loss. With increasing altitude, the gross ozone loss rate due to photolysis sharply decreases in absolute value to less than -0.05 ppbv h^{-1} above 8 km altitude. Between 6 and 10 km altitude, (total) gross ozone loss is of the order of -0.15 ppbv h^{-1}, mainly due to photolysis of O_3 while reaction of HO_2 with O_3 (-0.05 ppbv h^{-1}) and the reaction of OH with O_3 (-0.03 ppbv h^{-1}) are significantly smaller in absolute values. Above 10 km, gross ozone loss rate decreases to -0.03 to -0.05 ppbv h^{-1}. This is mainly due to a diminishing ozone loss via photolysis and reaction with H_2O at low humidity, leaving ozone loss by the reaction of O_3 with OH and HO_2 at -0.01 to 0.02 ppbv h^{-1} as major loss processes. Ozone loss rates observed above 10 km during CAFE-Africa have only little impact on NOPRs as they balance only about 10-20 % of the absolute value of concurrent gross ozone production rates at these altitudes.

The model generally reproduces the NOPR tendencies in gross production and loss as shown above, yielding net ozone destruction at a rate of –0.1 to –0.3 ppbv h^{-1} below 4 km altitude, which is significantly lower in absolute values than the measurement based calculation. This is due to a combination of a weaker loss term due to photolysis and of a larger production term due to the reaction of NO with HO_2 and CH_3O_2 represented in the model. The contribution of the reaction of NO with HO_2 represents a vertically constant value of about 0.2-0.3 ppbv h^{-1} with and a slightly larger production rate from the reaction of NO with CH_3O_2 at 0.05 to 0.1 ppbv h^{-1} than inferred from the measurements. Above 10 km altitude, EMAC reproduces the relative and absolute tendencies of the particular gross ozone loss rates remarkably well.

Our results are comparable to a previous study on NOPRs derived from in situ airborne observations at similar latitudes over the rainforest in South America (Bozem et al., 2017). Bozem et al. (2017) report net ozone destruction of -0.2 to -0.6 ppbv h^{-1} between 2 to 4 km and net ozone production between 7 and 9 km altitude with the transition from net ozone destruction to net ozone production occurring at 7 km, similar to our results. Below 6 km altitude gross ozone loss is dominated by photolysis in both studies (Bozem et al., 2017). Bozem et al. (2017) found net ozone production in the continental PBL layer. In this study O_3 destruction prevails, most likely due to the absence of large emission sources in the proximity of the Cape Verde Islands. In the marine boundary layer both studies tend towards net ozone destruction (Bozem et al., 2017).

Our results add to the understanding of photochemical net ozone production in the upper troposphere of the region. Using a photochemical trajectory model initiated by in situ measurements, Real et al. (2010) derived photochemical net ozone production rates of 2.6 ppbv/day over a period of 10 days downwind of West Africa. Our study supports the findings by Real et al. (2010) by underlining that photochemical ozone production in the upper troposphere over the tropics is positive at about

0.2-0.4 ppbv h^{-1}, which supports the concept of significant photochemical ozone production in the upper troposphere of the region. Note that during CAFE-Africa, measurements at low altitudes were generally performed over the Atlantic Ocean. Hence, we cannot compare to previous results from Saunois et al. (2009) reporting ozone production ranging from 0.25 to 0.75 ppbv h^{-1} in the continental boundary layer over West Africa.

In the following, we investigate the spatial distribution of NOPRs derived from measured and simulated data. Figure 6 shows the color-coded spatial, tropospheric distribution of upper tropospheric (> 12 km altitude) NOPRs calculated from observations (left plot) and model simulated data (middle plot). The right plot shows the spatial, average tropospheric distribution of the point-by-point NOPR(model)/NOPR(measurement) ratio. Note that a few single data points exceed the given color scales. Also note that NOPR calculations based on observational data are restricted to periods of simultaneous availability of a number measured species and parameters so that data gaps will be more likely than for spatial distributions of in situ NO or O_3.

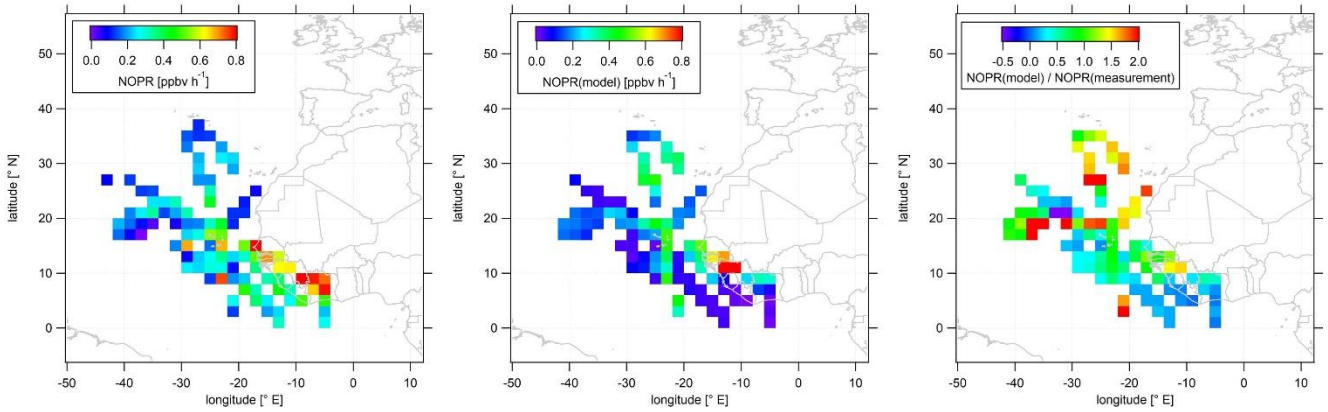

Figure 6: Color-coded spatial, tropospheric distributions of calculated NOPRs above 12 km during CAFE-Africa. The left and middle graphs show the spatial distribution of measured and simulated O_3, respectively. The right graph shows the spatial distribution of the NOPR(model)/NOPR(measurement) ratio. The figures have been filtered for stratospheric measurements by removing data points for which O_3 exceeds 100 ppbv.

The spatial distribution of NOPRs calculated based on measured data shows the already discussed, generally positive net ozone production tendencies in the upper tropical troposphere, but with distinct, characteristic regional features. While NOPRs are generally of the order of (0.2 ± 0.1) ppbv h^{-1} north of 16° N and west of -20° E, spatially averaged NOPRs in the area of the ITCZ are ~0.4 ppbv h^{-1} at several locations. Largest spatially averaged NOPRs based on the observations (> 0.8 ppbv h^{-1}) are found over tropical West Africa, mirroring strong NO enhancements (see Figure 3). Nevertheless, the highest NOPR values are inferred over the Ivory Coast although NO is lower than over Guinea or over Senegal, where the NOPR calculation yields comparable, but slightly smaller values. Over the Ivory Coast ozone formation is mainly driven by large HO_2 mixing ratios of up to 15-20 pptv (see supplement Figure S9 for spatial distributions of in situ measured and simulated OH and HO_2 data). Similar as for NO, the spatial distribution further suggest a longitudinal increase of NOPRs towards the West African coast

reflecting the general absence of LNO_x over oceanic areas and increased lightning flash rates over the tropical parts of West and Central Africa (Williams and Satori, 2004; Collier and Hughes, 2011).

The spatial distribution of NOPRs calculated based on simulated data largely follows the spatial distribution of simulated NO. Although the model indicates lowest NOPRs of less than 0.2 ppbv h^{-1} over most oceanic area, NOPRs derived from simulated data exhibit values of about 0.4 ppbv h^{-1} at several locations between -20 and -30° E, which correlate with enhancements in NO retrieved from EMAC. Over Africa, EMAC yields significant enhancements in NOPRs only between 10 and 14° N over Senegal, where NO is also enhanced.

The strong dependence of ozone formation on ambient NO concentrations for both measurement and model raises the question to which extent ozone formation was NO_x-limited. Figure 7 shows NOPRs calculated based on measured and simulated data in orange and blue, respectively, aggregated to a bin width of 0.025 ppbv of NO on the x-axis. There is only limited data coverage for measured NO above 0.325 ppbv and for simulated NO above 0.15 ppbv. See supplementary Table ST3 for the number of data points in each NO mixing ratio bin.

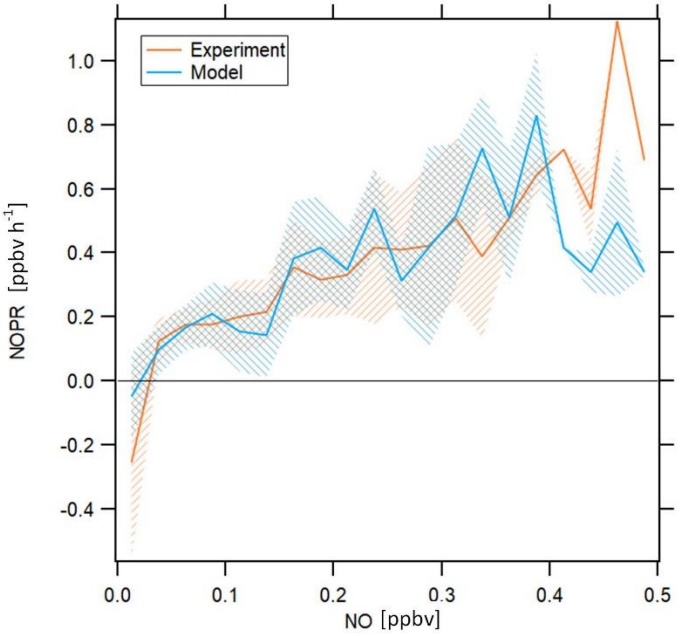

Figure 7: NOPRs derived from measured and simulated data as a function of NO mixing ratios. The orange and blue lines represent average profiles calculated based on measured and simulated data, respectively. The blue and orange shading represent ±1 standard deviations of the average lines. The profiles have been filtered for stratospheric measurements by removing data points for which O_3 exceeds 100 ppbv.

NOPRs derived from both observations and model simulations exhibit similar dependencies on ambient NO mixing ratios. Both measurements and model simulations show net ozone destruction below 30 and 20 pptv, respectively, and a nearly linear increase in NOPRs with increasing ambient NO mixing ratios above this threshold value, with an NOPR increase of 0.1 to

0.15 ppbv h^{-1} per 100 pptv increase in NO. Especially the NO compensation mixing ratio (for which ozone production equals ozone loss) reproduces results from previous studies remarkably well. Cantrell et al. (2003) report NO compensation mixing ratios between 10 and 30 pptv over the Pacific, depending on whether modelled or measured HO_2 and RO_2 is used. A study conducted by Zanis et al. (2000b) for the Swiss Alps also reports balance in ozone production for similar NO compensation mixing ratios. Due to low data coverage above 0.4 ppbv we cannot resolve with much certainty whether beyond this value the increase in NOPR will continue. Note that one possible limitation of this figure arises from the fact that the data aggregated in the respective NO mixing ratio bins stem from different atmospheric layers and origins, which causes the spiky signature of the profile for both measurement and model. However, both model simulations and observations indicate that O_3 in the upper troposphere in the tropics is NO_x-limited.

4 Conclusion

We presented in situ observations of NO, O_3 and a number of species involved in photochemical O_3 formation obtained in the upper tropical troposphere above the Atlantic Ocean and West Africa and compared these experimental results to simulated data retrieved from the global EMAC chemistry-climate model. Our results corroborate the overall eightfold increase of lightning flash rates over land compared to oceanic areas, and the associated NO production (Christian et al., 2003), as well as the notion that tropical Africa is one of the world's lightning hot spots (Williams and Satori, 2004) where large amounts of NO are naturally produced in the process of convection. Observed NO mixing ratios reveal a typical vertical average profile with lowest NO mixing ratios of less than 20 pptv in the free and middle troposphere and highest mixing ratios of 150-200 pptv above 12 km altitude. We report highest NO (> 0.4 ppbv) in the latitudinal range of the ITCZ (5° N to 15° N) and moreover over tropical West Africa. While we find overall good agreement when comparing average profiles of observed and EMAC model simulated NO, large deviations are sometimes found for point-to-point comparisons. The model does not reproduce the largest NO enhancements over West Africa and instead predicts highest NO values above 12 km altitude over large areas of the North Atlantic, which highlights the importance of an accurate representation of lightning NO in the model. Based on in situ measurements we found 60-70 ppbv O_3 in the upper tropical troposphere, which is well reproduced by the model. While the average vertical profile of NOPRs derived from in situ measurements varied vertically between -0.6 ppbv h^{-1} between 2 and 4 km altitude and 0.2-0.4 ppbv h^{-1} in the upper tropical troposphere, with a crossover in O_3 formation at around 8 km. A spatial distribution of NOPRs in the upper tropical troposphere created based on experimental in situ data indicates highest values over the West African continent, which is a result of large NO and HO_2 over the particular regions. Although the model simulations largely reproduce the observation-based NOPR values, this is at least partly due to compensating effects, e.g. low NO in the model is partly associated with enhanced HO_2 leading to locally increased NOPRs in the simulations. Overall both the observations and the model simulations exhibit a nearly linear dependency of NOPRs on ambient NO indicating NO_x-limitation of O_3-formation.

Data availability

Data used in this study are available to all scientists agreeing to the CAFE-Africa data protocol at https://doi.org/10.5281/zenodo.4442616.

Author contributions

IT, CMN, JL and HF designed the study. IT wrote the manuscript. IT and CMN processed and analyzed the data. IT and UP performed the NO, CO and CH_4 measurements during the campaign. IT processed the NO, CO and CH_4 data. DM, HH, MM and RR performed the OH and HO_2 measurements. BB supervised measurements and processed the actinic flux data. MZ supervised measurements and processed the water vapor data. FO supervised measurements and processed the O_3 data. AP generated model data.

Competing interest

The authors declare that they have no conflict of interest.

Acknowledgements

We acknowledge the collaborations with Forschungszentrum Jülich, Karlsruhe Institute of Technology, Heidelberg University, Deutsches Zentrum für Luft- und Raumfahrt and Wuppertal University during the CAFE-Africa campaign. We thank all involved in the CAFE-Africa project for a successful campaign.

Appendix: Acronyms and abbreviations

General

CAFE-Africa	**C**hemistry of the **A**tmosphere: **F**ield **E**xperiment in **Africa**
HALO	**H**igh **Al**titude and **Lo**ng-range research aircraft

Scientific

CLD	**C**hemi**l**uminescence **d**etector
ECHAM5	Fifth generation **E**uropean **C**entre **Ham**burg general circulation model
EMAC	**E**CHAM/**M**ESSy **A**tmospheric **C**hemistry **m**odel
FAIRO	**F**ast **Air**borne **O**zone Instrument
HORUS	**H**ydr**O**xyl **R**adical measurement **U**nit based on fluorescence **S**pectroscopy instrument
HO_x	OH + HO_2
ITCZ	**I**nter-**T**ropical **c**onvergence **z**one
LIF	**L**aser **i**nduced **f**luorescence
MBL	**M**arine **b**oundary **l**ayer
MESSy	**M**odular **E**arth **S**ubmodel **Sy**stem
MF	**M**easurement **f**light
NOPR	**N**et **o**zone **p**roduction **r**ate
NO_x	NO + NO_2
PBL	**P**lanetary **B**oundary **L**ayer
PSS	**P**hotostationary **s**teady **s**tate
QCLAS	**Q**uantum **c**ascade **l**aser **a**bsorption **s**pectroscopy
SHARC	**S**ophisticated **H**ygrometer for **A**tmospheric **R**esear**C**h)
SLM	**S**tandard **l**itre per **m**inute

	TDL	**T**unable **d**iode **l**aser
	TMU	**T**otal **m**easurement **u**ncertainty
	T/O	**T**ake **o**ff
	VOC	**V**olatile **o**rganic **c**ompound
560	UTC	**C**oordinated **u**niversal **t**ime
	UTLS	**U**pper **t**roposphere/**l**ower **s**tratosphere

References

Aghedo, A. M., Schultz, M. G., and Rast, S.: The influence of African air pollution on regional and global tropospheric ozone, *Atmos. Chem. Phys.*, **7**, 1193-1212, https://doi.org/ 10.5194/acp-7-1193-2007, 2007.

Atkinson, R., Baulch, D. L., Cox, R. A., Crowley, J. N., Hampson, R. F., Hynes, R. G., Jenkin, M. E., Rossi, M. J., and Troe, J.: Evaluated kinetic and photochemical data for atmospheric chemistry: volume I gas phase reactions of O_x, HO_x, NO_x and SO_x species, 2004, *Atmos. Chem. Phys.*, **4**, 1461-1738, https://doi:10.5194/acp-4-1461-2004, 2004.

Atkinson, R., Baulch, D. L., Cox, R. A., Crowley, J. N., Hampson, R. F., Hynes, R. G., Jenkin, M. E., Rossi, M. J., and Troe, J.: Evaluated kinetic and photochemical data for atmospheric chemistry: volume I gas phase reactions of organic species, *Atmos. Chem. Phys.*, **6**, 3625-4055, https://doi:10.5194/acp-6-3625-2006, 2006.

Beirle, S., Huntrieser, H., and Wagner, T.: Direct satellite observations of lightning-produced NO_x, *Atmos. Chem. Phys.*, **10**, 10965-10986, https://doi.org/10.5194/amt-10-10965-2010, 2010.

Berrisford, P., Dee, D. P. K. F., Fielding, K., Fuentes, M., Kallberg, P., Kobayashi, S., and Uppala, S.: The ERA-Interim archive, *ERA report series*, No. 1 ECMWF: Reading, UK, 2009.

Bohn, B. and Lohse, I.: Calibration and evaluation of CCD spectroradiometers for ground-based and airborne measurements of spectral actinic flux densities, *Atmos. Meas. Tech.*, **10**, 3151–3174, https://doi.org/10.5194/amt-10-3151-2017, 2017.

Bourgeois, I., Peischl, J., Thompson, C. R., Aikin, K. C., Campos, T., Clark, H., Commane, R., Daube, B., Diskin, G. W., Elkins, J. W., Gao, R.-S., Gaudel, A., Hintsa, E. J., Johnson, B. J., Kivi, R., McKain, K., Moore, F. L., Parrish, D. D., Querel, R., Ray, E., Sánchez, R., Sweeney, C., Tarasick, D. W., Thompson, A. M., Thouret, V., Witte, J. C., Wofsy, S. C., and Ryerson, T. B.: Global-scale distribution of ozone in the remote troposphere from the ATom and HIPPO airborne field missions, *Atmos. Chem. Phys.*, **20**, 10611–10635, https://doi.org/10.5194/acp-20-10611-2020, 2020.

Bozem H., Butler T. M., Lawrence M. G., Harder H., Martinez M., Kubistin D., Lelieveld J., Fischer H.: Chemical processes related to net ozone tendencies in the free troposphere, *Atmos. Chem. Phys.*, **17**, 10565-10582, https://doi.org/10.5194/acp-17-10565-2017, 2017.

Cantrell, C. A., Edwards, G. D., Stephens, S., Mauldin, R. L., Zondlo, M. A., Kosciuch, E., Eisele, F. L., Shetter, R. E., Lefer, B. L., Hall, S., Flocke, F., Weinheimer, A., Fried, A., Apel, E., Kondo, Y., Blake, D. R., Blake, N. J., Simpson, I. J., Bandy, A. R., Thornton, D. C., Heikes, B. G., Singh, H. B., Brune, W. H., Harder, H., Martinez, M., Jacob, D. J., Avery, M. A., Barrick, J. D., Sachse, G. W., Olson, J. R., Crawford, J. H., and Clarke, A. D.: Peroxy radical behavior during the Transport

and Chemical Evolution over the Pacific (TRACE-P) campaign as measured aboard the NASA P-3B aircraft, *J. Geophys. Res.*, **108**, D20, https://doi.org/10.1029/2003JD003674, 2003.

Christian, H. J., Blakeslee, R. J., Boccippio, D. J., Boeck, W. L., Buechler, D. E., Driscoll, K. T., Goodman, S. J., Hall, J. M., Koshak, W. J., Mach, D. M., and Stewart, M. F.: Global frequency and distribution of lightning as observed from space by the Optical Transient Detector, *J. Geophys. Res.*, **108**, D1, 4005, https://doi.org/10.1029/2002DJ002347, 2003.

Collier, A. B., and Hughes, A. R. W.: A harmonic model for the temporal lightning activity over Africa, *J. Geophys. Res.*, **116**, D05105, https://doi.org/10.1029/2010JD014455, 2011.

Crippa, M., Guizzardi, D., Muntean, M., Schaaf, E., Dentener,F., van Aardenne, J. A., Monni, S., Doering, U., Olivier,J. G. J., Pagliari, V., and Janssens-Maenhout, G.: Gridded emissions of air pollutants for the period 1970–2012 within EDGAR v4.3.2, *Earth Syst. Sci. Data*, **10**, 1987-2013, https://doi.org/10.5194/essd-10-1987-2018, https://www.earth-syst-sci-data.net/10/1987/2018/, 2018.

Crutzen. P. J.: Photochemical reactions initiated by and influencing ozone in unpolluted tropospheric air, *Tellus*, **26**, 48-57, https://doi.org/10.1111/j.2153-3490.1974.tb01951.x, 1974.

Dentener, F., Stevenson, D., Cofala, J., Mechler, R., Amann, M., Bergamaschi, P., Raes, F., and Derwent, R.: The impact of air pollutant and methane emission controls on tropospheric ozone and radiative forcing: CTM calculations for the period 1990-2030, *Atmos. Chem. Phys.*, **5**, 1731-1755, https://doi.org/10.5194/acp-5-1731-2005, 2005.

Duncan, B. N., Yoshida, Y., Olson, J. R., Sillman, S., Martin, R. V., Lamsal, L., Hu, Y., Pickering, K. E., Retscher, C., Allen, D. J., Crawford, J. H.: Application of OMI observations to a space-based indicator of NO_x and VOC controls on surface ozone formation, *J. Atmos. Env.*, **44**, 2213-2223, doi:10.1016/j.atmosenv.2010.03.010, 2010.

Fiore, A. M., Jacob, D. J., Bey. I., Yantosca, R. M., Field, B. D., Fusco, A. C., and Wilkinson, J. G.: Background ozone over the United States in summer: Origin, trend, and contribution to pollution episodes, *J. Geophys. Res.*, **107**, D15, 4275, https://doi.org/10.1029/2001JD000982, 2002.

Galanter, M., Levy, H., Carmichael, G. R.: Impacts of biomass burning on tropospheric CO, NO_x and O_3, *J. Geophys. Res.*, **105**, D5, 6633-6653, https://doi.org/10.1029/1999JD901113, 2000.

Grewe, V., Brunner, D., Dameris, M., Grenfell, J., Hein, R., Shindell, D., and Staehelin, J.: Origin and variability of upper tropospheric nitrogen oxides and ozone at northern mid-latitudes, *Atmos. Environ.*, **35**, 3421–3433, https://doi.org/10.1016/S1352-2310(01)00134-0, 2001.

Hosaynali Beygi, Z., Fischer, H., Harder, H. D., Martinez, M., Sander, R., Williams, J., Brookes, D. M., Monks, P. S., Lelieveld, J.: Oxidation photochemistry in the Southern Atlantic boundary layer: unexpected deviations of photochemical steady state, *Atmos. Chem. Phys.*, **11**, 8497-8513, https://doi:10.5194/acp-11-8497-2011, 2011

Jaffe, D. A., Cooper, O. R., Fiore, A. M., Henderson, B. H., Tonnesen, G. S., Russell, A. G., Henze, D. K., Langford, A. O., Lin, M., and Moore, T.: Scientific assessment of background ozone over the US.: Implications for air quality management, *Elem. Sci. Anth.*, **6**, 56, https://doi.org.10.1526/elementa.309, 2018.

Jeucken, A. B. M., Siegmund, P. C., and Heijboer, L. C.: On the potential of assimilating meteorological analyses in a global climate model for the purpose of model validation, *J. Geophys, Res.*, **101**, D12, 16939-16950, https://doi.org/10.1029/96JD01218, 1996

Jöckel, P., Kerkweg A., Pozzer, A., Sander, R., Tost, H., Riede, H., Baumgartner, A., Gromov, S., and Kern, B.: Development of cycle 2 of the Modular Earth Submodel System (MESSy2), *Geosci. Model Dev.*, **3**, 717-752, https://doi.org/10.5194/gmd-3-717-2010, 2010.

Kaiser, J. W., Heil, A., Andreae, M. O., Benedetti, A., Chubarova, N., Jones, L., Morcrette, J.-J., Razinger, M., Schultz, M. G., Suttie, M., and van der Werl, G. R.: Biomass burning emissions estimated with a global fire assimilation system based on observed fire radiative power, *Biogeosciences*, **9**, 527-554, https://doi.org/10.5194/bg-9-527-2012, 2012.

Kerkweg, A., Buchholz, J., Ganzeveld, L., Pozzer, A., Tost, H., and Jöckel, P.: Technical Note: An implementation of the dry removal processes DRY DEPosition and SEDImentation in the Modular Earth Submodel System (MESSy), *Atmos. Chem. Phys.*, **6**, 4617–4632, https://doi.org/10.5194/acp-6-4617-2006, 2006.

Kley, D., Drummond, J. W., McFarland, M., and Liu, S. C.: Tropospheric profiles of NO_x, *J. Geophys. Res.*, **86**, C4, 3153-3161, https://doi.org/10.1029/JC086iC04p03153, 1981.

Krautstrunk, M., Giez, A.: The Transition From FALCON to HALO Era Airborne Atmospheric Research, in: Schumann U. (eds) Atmospheric Physics. Research Topics in Aerospace, *Springer*, Berlin, Heidelberg, https://doi.org/10.1007/978-3-642-30183-4_37, 2012.

Lelieveld, J., van Aardenne, J., Fischer, H., de Reus, M., Williams, J., and Winkler, P.: Increasing Ozone over the Atlantic Ocean, *Science*, **304**, Issue 5676, 1483-1487, https://doi.org/10.1126/science.1096777, 2004.

Lelieveld, J., Hoor, P., Jöckel, P., Pozzer, A., Hadjinicolaou, P., Cammas, J.-P., and Beirle, S.: Severe ozone air pollution in the Persian Gulf region, *Atmos. Chem. Phys.*, **9**, 1393–1406, https://doi.org/10.5194/acp-9-1393-2009, 2009.

Lin, X., Trainer, M., and Liu, S. C.: On the nonlinearity of the tropospheric ozone production, *J. Geophys. Res.*, **93**, D12, https://doi.org/10.1029/JD093iD12p15879, 1988.

Lu, K., Zhang, Y., Su, H., Brauers, T., Chou, C. C., Hofzumahaus, A., Liu, S. C., Kita, K., Kondo, Y., Shao, M., Wahner, A., Wang, J., Wang, X., and Zhu, T.: Oxidant (O_3 + NO_2) production processes and formation regimes in Beijing, *J. Geophys. Res.*, **115**, D07303, https://doi.org/10.1029/2009JD012714, 2010.

Mannschreck, K., Gilge, S., Plass-Duelmer, C., Fricke, W., and Berresheim, H.: Assessment of the applicability of NO-NO_2-O_3 photostationary state to long-term measurements at the Hohenpeissenberg GAW Station, Germany, *Atmos. Chem. Phys.*, **4**, 1265-1277, https://doi.org/10.5194/acp-4-1265-2004, 2004.

Marno, D., Ernest, C., Hens, K., Javed, U., Klimach, T., Martinez, M., Rudolf, M., Lelieveld, J., and Harder, H.: Calibration of an airborne HO_x instrument using the All Pressure Altitude-based Calibrator for HO_x Experimentation (APACHE), *Atmos. Meas. Tech.*, **13**, 2711-2731, https://doi.org/10.5194/amt-13-2711-2020, 2020.

Miyazaki, K., Eskes, H. J., Sudo, K., and Zhang, C.: Global lightning NO_x production estimated by an assimilation of multiple satellite data sets, *Atmos. Chem. Phys.*, **14**, 3277–3305, https://doi.org/10.5194/acp-14-3277-2014, 2014.

Miyazaki, K., Eskes, H., Sudo, K., Folkert Boersma, K., Bowman, K., and Kanaya, Y.: Decadal changes in global surface NO_x emissions from multi-constituent satellite data assimilation, *Atmos. Chem. Phys.*, **17**, 807-837, https://doi.org/10.5194/acp-17-807-2017, 2017.

Nussbaumer, C. M., and Cohen, R. C.: The role of temperature and NO_x in ozone trends in the Los Angeles Basin, *Environ. Sci. Technol.*, **54**, 15652-15659, https://doi.org/10.1021/acs.est.0c04910, 2020.

Prather, M. J., Zhu, X., Tang, Q., Hsu, J., and Neu, J. L.: An atmospheric chemist in search of the tropopause, *J. Geophys. Res.*, **116**, D04306, https://doi.org/10.1029/2010JD014939, 2011.

Pusede, S. E., Steiner, A., and Cohen, R. C.: Temperature and recent trends in the chemistry of continental surface ozone, *Chem. Rev.*, **115**, 10, 3898-3918, https://doi.org/10.1021/cr5006815, 2015.

Real, E., Orlandi, E., Law, K. S., Fierli, F., Josset, D., Cairo, F., Schlager, H., Borrmann, S., Kunkel, D., Volk, C. M., McQuaid, J. B., Stewart, D. J., Lee, J., Lewis, A. C., Hopkins, J. R., Ravegnani, F., Ulanovski, A., and Liousse, C.: Cross-hemispheric transport of central African biomass burning pollutants: implications for downwind ozone production, *Atmos. Chem. Phys.*, **10**, 3027–3046, https://doi.org/10.5194/acp-10-3027-2010, 2010.

Reed, C., Evans, M. J., Carlo, P. D., Lee, J. D., Carpenter, L. J.: Interferences in photolytic NO_2 measurements: explanation for an apparent missing oxidant?, *Atmos. Chem. Phys.*, **16**, 4707-4724, https://doi:10.5194/acp-16-4707-2016, 2016.

Ridley, B. A., and Howlett, L. C.: An instrument for nitric oxide measurements in the stratosphere, *Rev. Sci. Instrum.*, **45**, 6, https://doi.org/10.1063/1.1686726, 1974.

Roeckner, E., Brokopf, R., Esch, M., Giorgetta, M., Hagemann, S., Kornblueh, L., Manzini, E., Schlese, U., and Schulzweida, U.: Sensitivity of Simulated Climate to Horizontal and Vertical Resolution in the ECHAM5 Atmosphere Model, *J. Climate*, **19**, 3771-3791, https://doi.org/10.1175/JCLI3824.1, 2006.

Ryerson, T.B., Williams, E. J., Fehsenfeld, F. C.: An efficient photolysis system for fast-response NO_2 measurements, *J. Geophys. Res.*, **105**, 447-461, https://doi.org/10.1029/2000JD900389, 2002.

Sander, R., Jöckel, P., Kirner, O., Kunert, A. T., Landgraf, J., and Pozzer, A.: The photolysis module JVAL-14, compatible with the MESSy standard, and the JVal PreProcessor (JVPP), *Geosci. Model Dev.*, **7**, 2653–2662, https://doi.org/10.5194/gmd-7-2653-2014, 2014.

Saunois, M., Reeves, C. E., Mari, C. H., Murphy, J. G., Stewart, D. J., Mills, G. P., Oram, D. E., and Purvis, R. M.: Factors controlling the distribution of ozone in the West African lower troposphere during the AMMA (African Monsoon Multidisciplinary Analysis) wet season campaign, *Atmos. Chem. Phys.*, 9, 6135-6155, https://doi.org/10.5194/acp-9-6135-2009, 2009.

Sander, R., Baumgartner, A., Cabrera-Perez, D., Frank, F., Gromov, S., Grooß, J.-U., Harder, H., Huijnen, V., Jöckel, P., Karydis, V. A., Niemeyer, K. E., Pozzer, A., Riede, H., Schultz, M. G., Taraborrelli, D., and Tauer, S.: The community atmospheric chemistry box model CAABA/MECCA-4.0, *Geosci. Model Dev.*, **12**, 1365-1385, https://doi.org/10.5194/gmd-12-1365-2019, 2019.

Schiller, C. I., Bozem, H., Gurk, C., Parchatka, U., Königstedt, R., Harris, G. W., Lelieveld, J., and Fischer, H.: Applications of quantum cascade lasers for sensitive trace gas measurements of CO, CH_4, N_2O, and HCHO, *Appl. Phys. B*, **92**, 419–430, https://doi.org/10.1007/s00340-008-3125-0, 2008.

Schroeder, J. S., Crawford, J. H., Fried, A., Walega, J., Weinheimer, A., Wisthaler, A., Müller, M., Mikoviny, T., Chen, G., Shook, M., Blake, D. R., and Tonnesen, G. S.: New insights into the column CH_2O/NO_2 ratio as an indicator of near-surface ozone sensitivity, *J. Geophys. Res. Atmos.*, **122**, 8885-8907, https://doi.org/10.1002/2017JD026781, 2017.

Sillman, S., Al-Wali, K., Marsik, F. J., Nowacki, P., Samson, P. J., Rodgers, M. O., Garland, L. J., Martinez, J. E., Stoneking, C., Imhoff, R., Lee, J. H., Newman, L., Weinstein-Lloyd, J., and Aneja, V.: Photochemistry of ozone formation in Atlanta, GA - models and measurements, *Atmos. Environ.*, **29**, 21, 3055-3066., doi:10.1016/1352-2310(95)00217-M, 1995.

Sillman, S., Vautard, R., Menut, L., and Kley, D.: O_3-NO_x-VOC sensitivity and NO_x-VOC indicators in Paris: Results from models and Atmospheric Pollution Over the Paris Area (ESQUIF) measurements, *J. Geophys. Res.*, **108**, D17, https://doi.org/10.1029/2002JD001561, 2003.

Silvern, R. F., Jacob, D. J., Travis, K. R., Sherwen, T., Evans, M. J., Cohen, R. C., Laughner, J. L., Hall, S. R., Ullmann, K., Crounse, J. D., Wennberg, P. O., Peischl, J., Pollack, I. B.: Observed NO/NO_2 ratios in the upper troposphere imply errors in NO-NO_2-O_3 cycling kinetics or an unaccounted NO_x reservoir, *Geophys. Res. Lett.*, **45**, 4466-4474, https://doi.org/10.1029/2018GL077728, 2018.

Tadic, I., Parchatka, U., Königstedt, R., Fischer, H.: In-flight stability of quantum cascade laser-based infrared absorption spectroscopy measurements of atmospheric carbon monoxide, *Appl. Phys. B*, **123**, 146, https://doi.org/10.1007/s00340-017-6721-z, 2017.

Tadic, I., Crowley, J. N., Dienhart, D., Eger, P., Harder, H., Hottmann, B., Martinez, M., Parchatka, U., Paris, J.-D., Pozzer, A., Rohloff, R., Schuladen, J., Shenolikar, J., Tauer, S., Lelieveld, J., and Fischer, H.: Net ozone production and its relationship to nitrogen oxides and volatile organic compounds in the marine boundary layer around the Arabian Peninsula, *Atmos. Chem. Phys.*, **20**, 6769-6787, https://doi.org/10.5194/acp-20-6769-2020, 2020.

Thornton, J. A., Wooldridge, P. J., Cohen, R. C., Martinez, M., Harder, H., Brune, W. H., Williams, E. J., Roberts, J. M., Fehsenfeld, F. C., Hall, S. R., Shetter, R. E., Wert, B. P., and Fried, A.: Ozone production rates as a function of NO_x abundances and HO_x production rates in the Nashville urban plume, *J. Geophys. Res.*, **107**, D12, https://doi.org/10.1029/2001JD000932, 2002.

Tost, H., Jöckel, P., Kerkweg, A., Sander, R., and Lelieveld, J.: Technical Note: A new comprehensive SCAVenging submodel for global atmospheric chemistry modelling, *Atmos. Chem. Phys.*,**6**, 565–574, https://doi.org/10.5194/acp-6-565-2006, 2006.

Tost, H., Jöckel, P., and Lelieveld, J.: Lightning and convection parameterisations – uncertainties in global modelling, *Atmos. Chem. Phys.*, **7**, 4553-4568, https://doi.org/10.5194/acp-7-4553-2007, 2007.

West, J. J., and Fiore, A. M.: Management of tropospheric ozone by reducing methane emissions, *Environ. Sci. Technol.*, **39**, 13, 4685-4691, https://doi.org/10.1021/es048629f, 2005.

Williams, E. R. and Satori, G.: Lightning, thermodynamic and hydrological comparison of the two tropical continental chimneys, *J. Atmos. Sol.*, **66**, 13-14, 1213-1231, https://doi.org/10.1016/j.jastp.2004.05.015, 2004

Xu, W., and Zipser, E. J.: Properties of deep convection in tropical continental, monsoon, and oceanic rainfall regimes, *Geophys. Res. Lett.*, **39**, L07802, https://doi.org/10.1029/2012GL051242, 2012.

Yienger, J. and Levy II, H.: Empirical model of global soil-biogenic NO_x emissions, *J. Geophys. Res.*, **100**, 11 447–11 464, https://doi.org/10.1029/95JD00370, 1995.

Zahn, A., Weppner, J., Schlote-Holubek, K., Burger, B., Kühner, T., and Franke, H.: A fast and precise chemiluminescence ozone detector for eddy flux and airborne application, *Atmos. Meas. Tech.*, **5**, 363-375, https://doi.org/10.5194/amt-5-363-2012, 2012.

Zanis, P., Monks, P. S., Schuepbach, E., and Penkett, S. A.: The Role of In Situ Photochemistry in the Control of Ozone during Spring at the Jungfraujoch (3,580 m asl) – Comparison of Model Results with Measurements, *J. Atmos. Chem.*, **37**, 1-27, https://doi.org/10.1023/A:1006349926926, 2000a.

Zanis, P., Monks, P. S., Schuepbach, E., Carpenter, L. J., Green, T. J., Mills, G. P., Bauguitte, S., and Penkett, S. A.: In situ ozone production under free tropospheric conditions during FREETEX '98 in the Swiss Alps, J. Geophys. Res., 105, D19, https://doi.org/10.1029/2000JD900229, 2000b.

Zipser, E. J.: Deep Cumulonimbus Cloud System in the Tropics with and without Lightning, *Mon. Wea. Rev.*, **122**, 1837-1851, https://doi.org/10.1175/1520-0493(1994)122<1837:DCCSIT>2.0.CO;2, 1994.

Supplement of

Central role of nitric oxide in ozone production in the upper tropical troposphere over the Atlantic Ocean and West Africa

Ivan Tadic[1], Clara M. Nussbaumer[1], Birger Bohn[2], Hartwig Harder[1], Daniel Marno[1], Monica Martinez[1], Florian Obersteiner[3], Uwe Parchatka[1], Andrea Pozzer[1,4], Roland Rohloff[1], Martin Zöger[5], Jos Lelieveld[1,6] and Horst Fischer[1]

[1]Atmospheric Chemistry Department, Max Planck Institute for Chemistry, Mainz, Germany
[2]Institute of Energy and Climate Research, IEK-8: Troposphere, Forschungszentrum Jülich GmbH, Jülich, Germany
[3]Karlsruhe Institute of Technology, Karlsruhe, Germany
[4]Earth System Physics section, The Abdus Salam International Centre for Theoretical Physics, Trieste, Italy
[5]Flight Experiments, German Aerospace Center (DLR), Oberpfaffenhofen, Germany
[6]Climate and Atmosphere Research Center, The Cyprus Institute, Nicosia, Cyprus

Correspondence: Ivan Tadic (i.tadic@mpic.de) or Horst Fischer (horst.fischer@mpic.de)

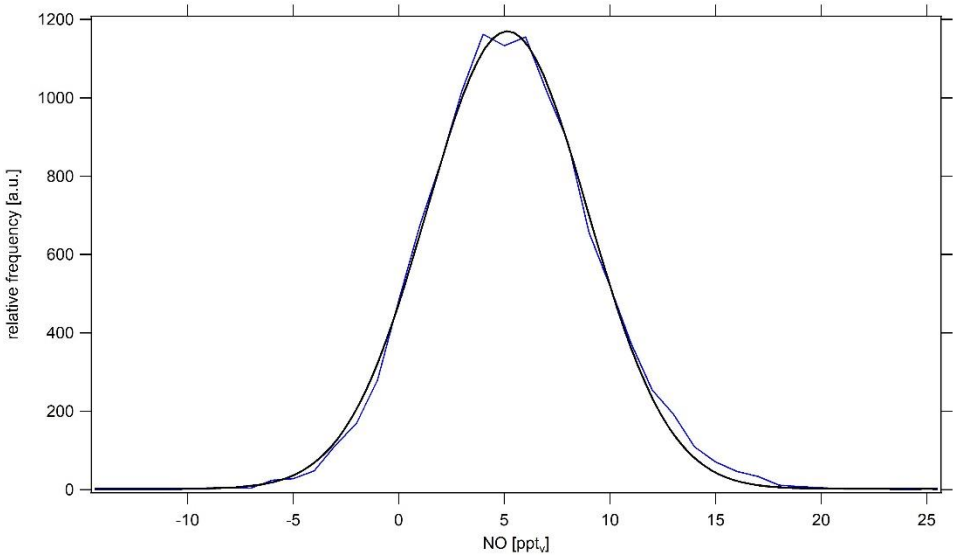

Figure S1: Distribution of in situ NO data (1 s time resolution) obtained during night-time during MF11. Note that the data have not been corrected for the residual instrumental background. The black trace shows a Gaussian fit to the obtained distribution from which the LOD and residual background corrections were retrieved.

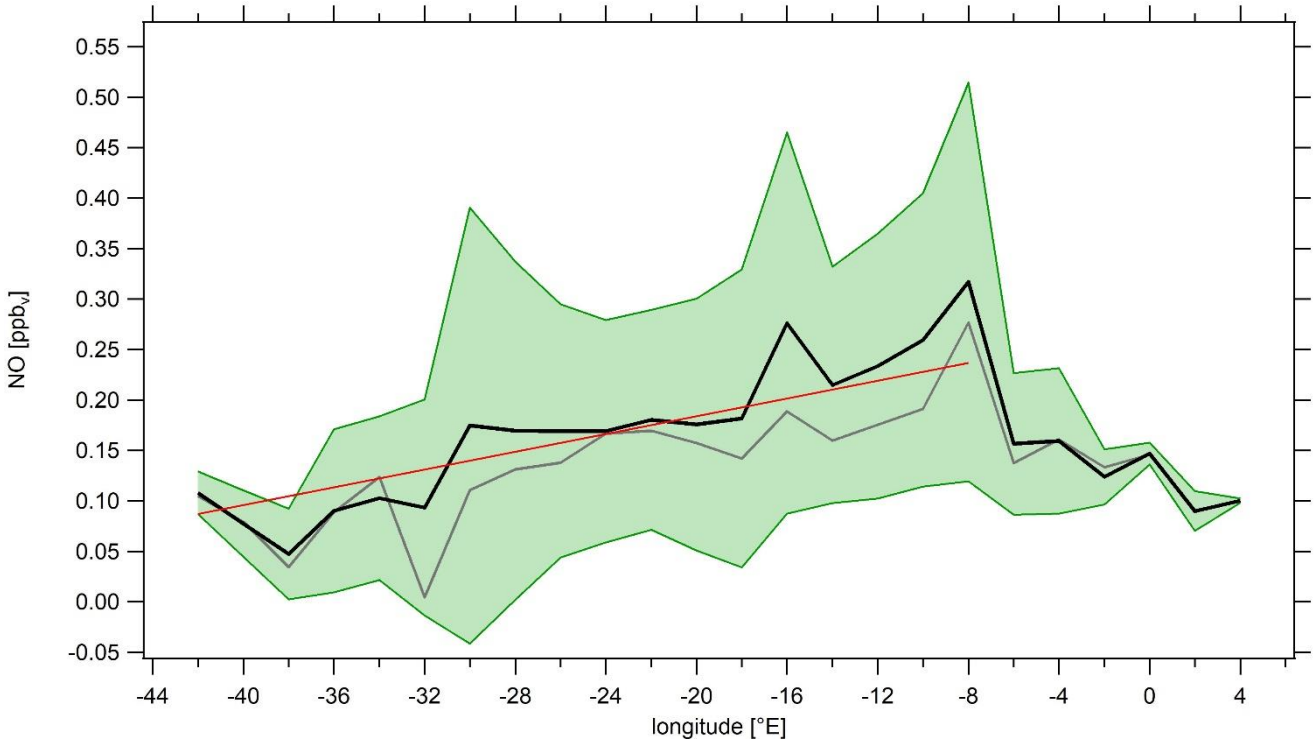

Figure S2: Longitudinal profile of NO data obtained above 12 km at a longitudinal resolution of 2 degree. The black and grey traces represent the average and median longitudinal profile, respectively. The green background represents ±1 standard deviation of the average profile. A linear fit to the averaged data in the interval from -42° E to -8° E (least squares method, weighted by standard deviation of the respective average) yields a longitudinal increase in NO of about 4.4 pptv per degree longitude towards the West African continent. Note that data obtained at latitudes eastbound of -4° N were observed over the European continent.

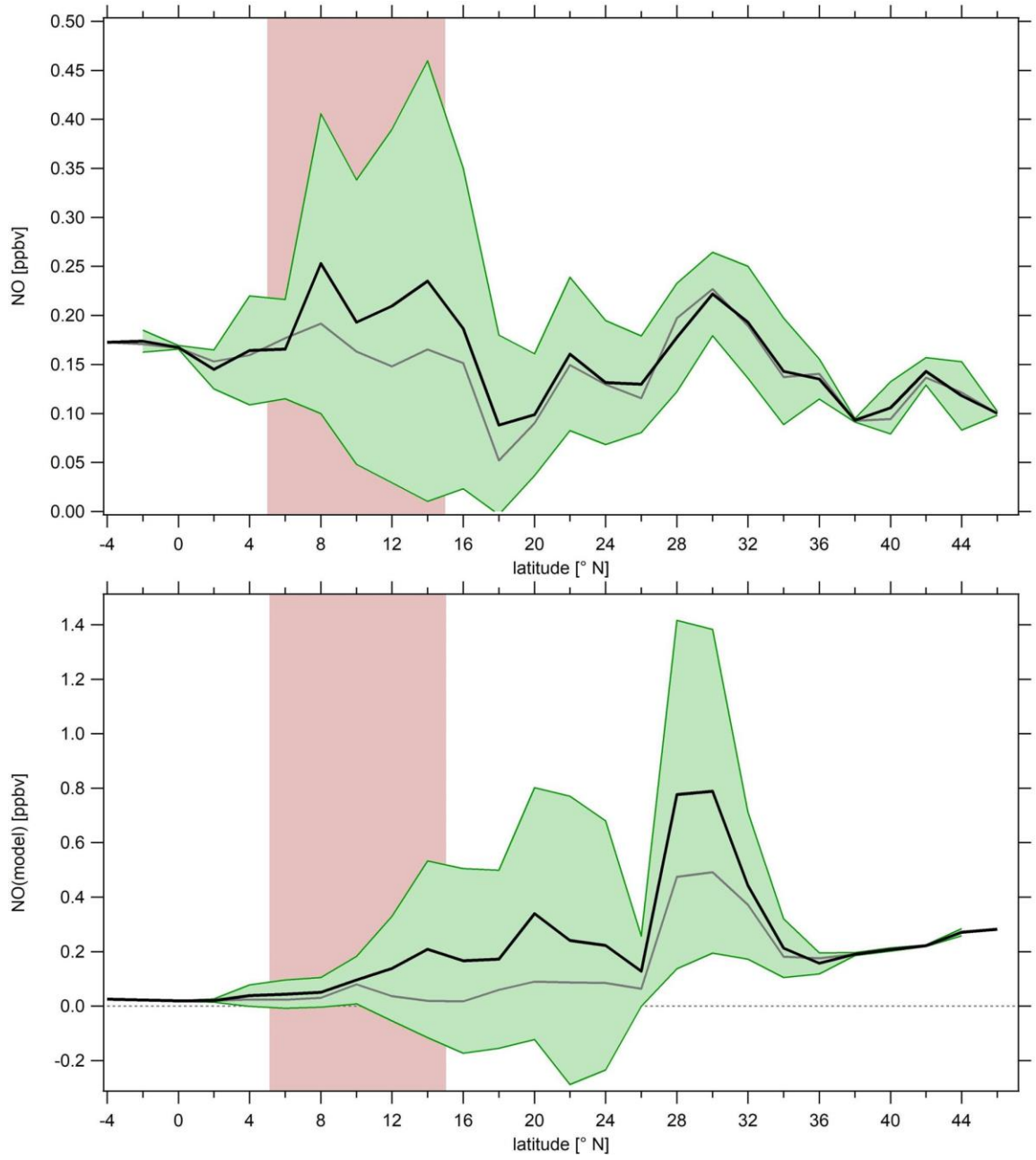

765 **Figure S3: Latitudinal profile of measured (upper plot) and simulated (lower plot) NO data obtained above 12 km at a latitudinal resolution of 2 degree. The black and grey traces represent the average and median latitudinal profile, respectively. The green background represents ±1 standard deviation of the average profile. The red box in the background indicates the supposable location of the ITCZ during August and September. The profiles were filtered for stratospheric measurements by removing data for which concurrent O_3 is > 100 ppbv.**

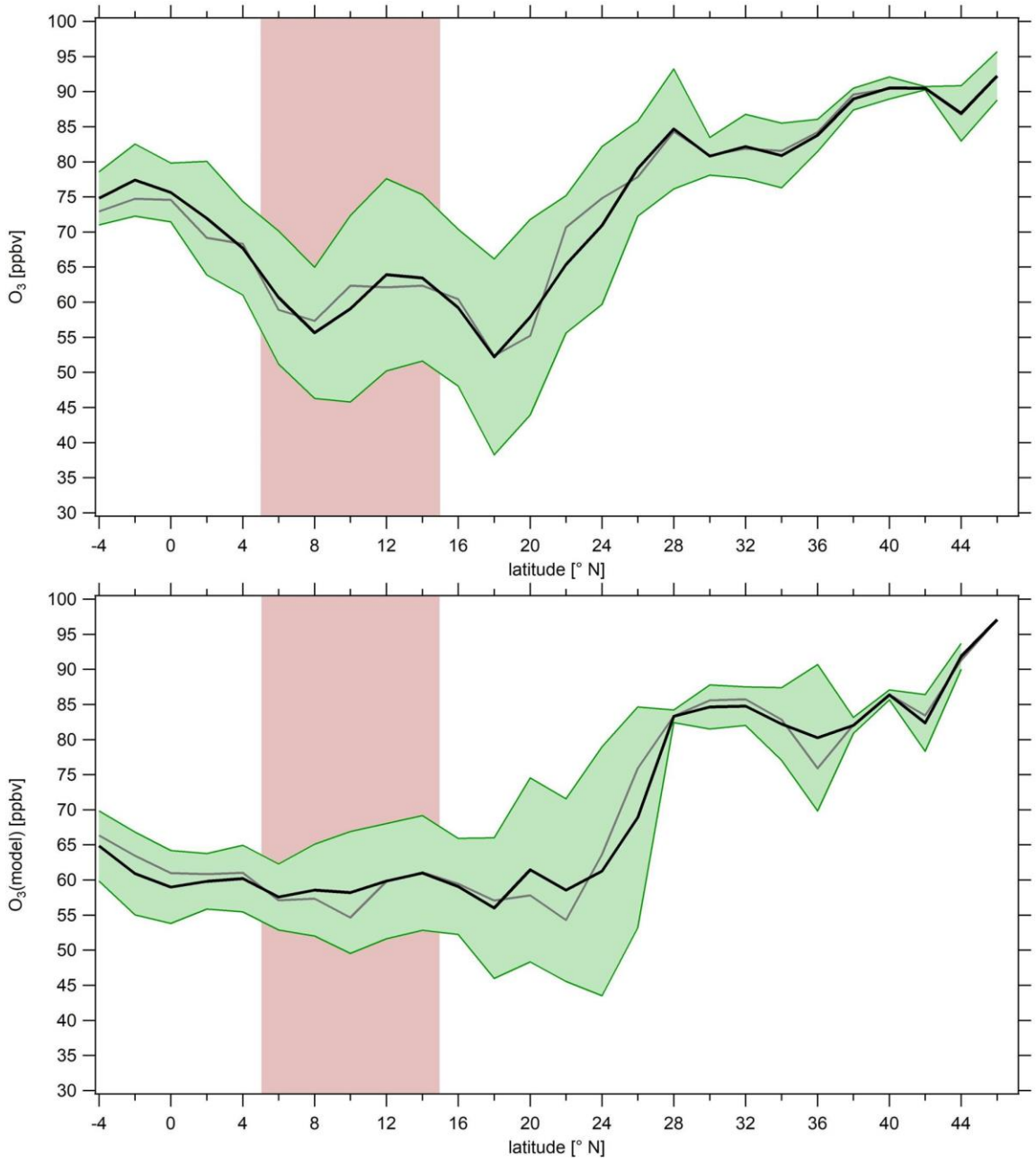

Figure S4: Latitudinal profile of measured (upper plot) and simulated (lower plot) O_3 data obtained above 12 km at a latitudinal resolution of 2 degree. The black and grey traces represent the average and median latitudinal profile, respectively. The green background represents ± 1 standard deviation of the average profile. The red box in the background indicates the supposable location of the ITCZ during August and September. The profiles were filtered for stratospheric measurements by removing data for which concurrent O_3 is > 100 ppbv.

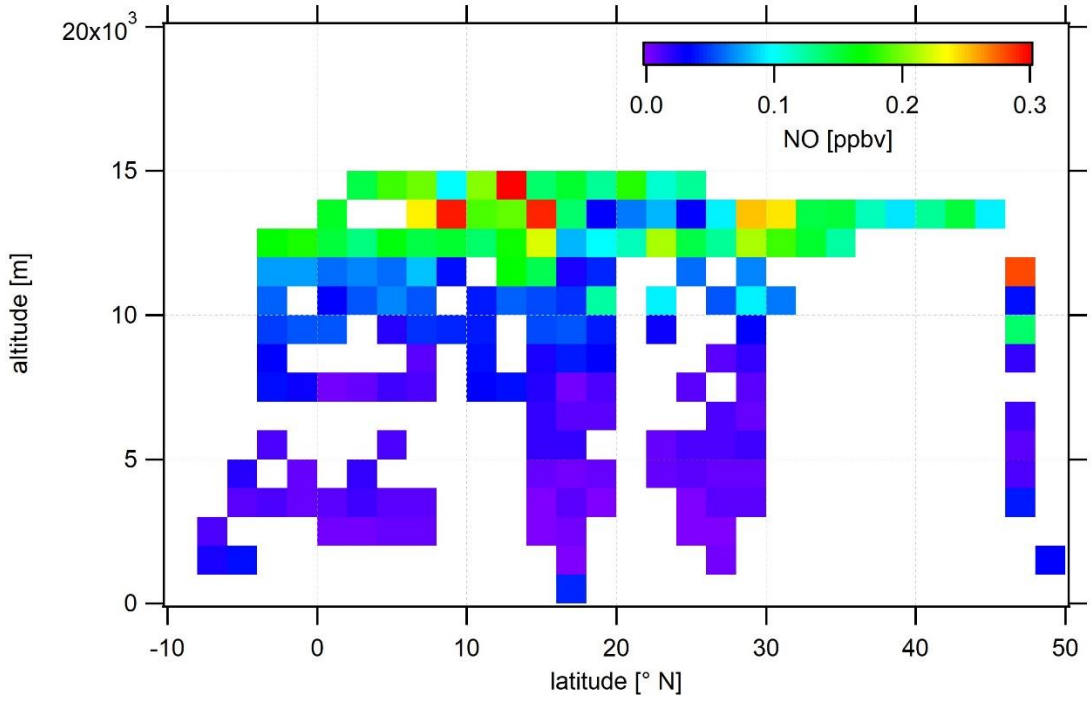

Figure S5: Latitudinal/altitudinal distribution of measured, tropospheric NO obtained during the campaign. The data have been aggregated and averaged over a grid width of 2 degree latitude and 1 km altitude.

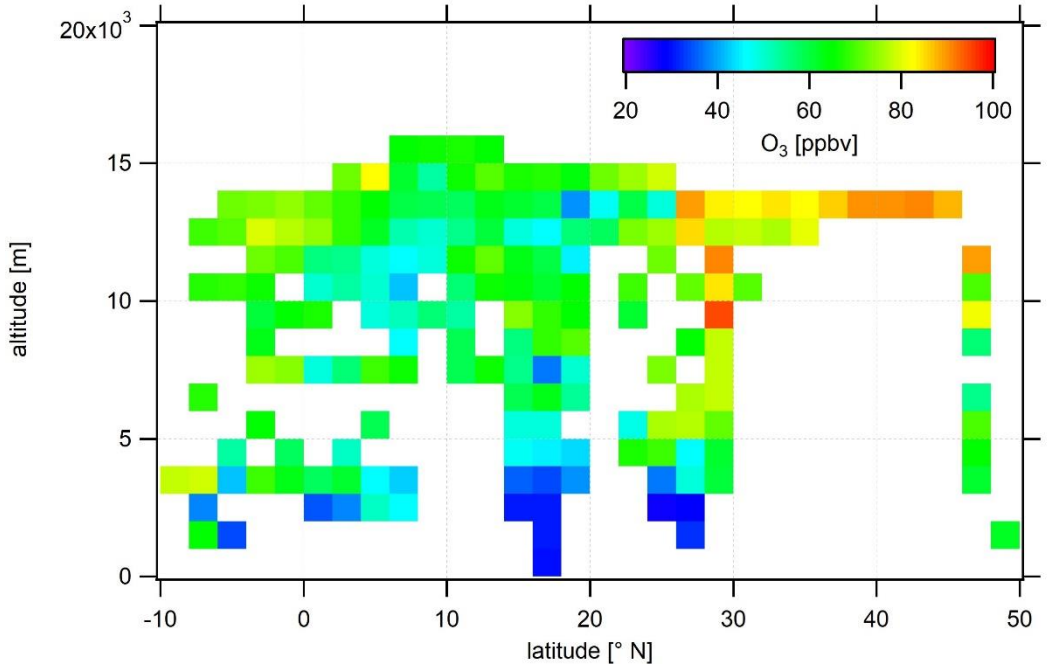

Figure S6: Latitudinal/altitudinal distribution of measured, tropospheric O_3 obtained during the campaign. The data have been aggregated and averaged over a grid width of degree latitude and 1 km altitude.

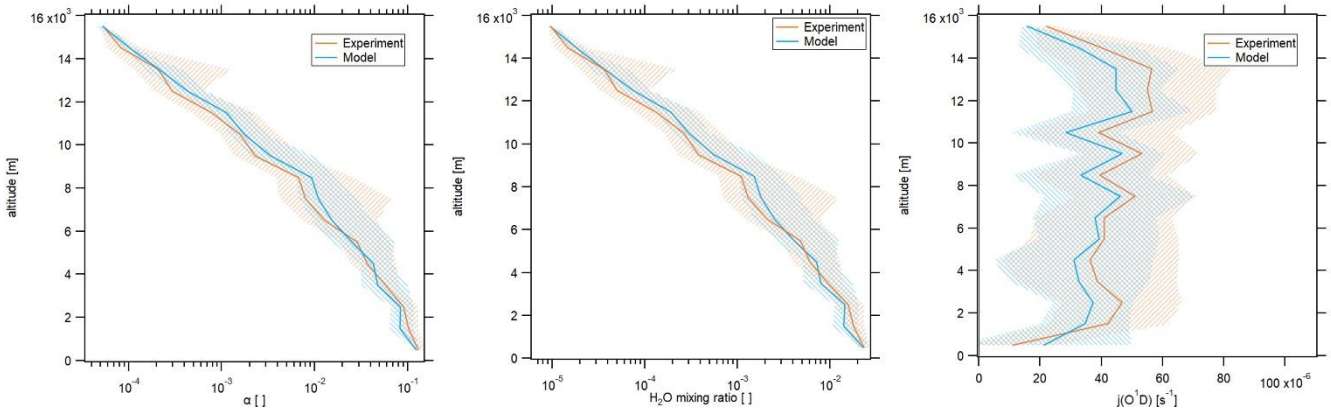

Figure S7: Vertical, tropospheric profile of α calculated based on measured and simulated data during CAFE-Africa (left graph). Vertical, tropospheric profile of H_2O mixing ratios calculated based on measured and simulated data during CAFE-Africa (middle graph). Vertical, tropospheric profile of $j(O^1D)$ (measured and simulated) obtained during CAFE-Africa (right graph). The orange and blue traces represent measured and simulated results, respectively.

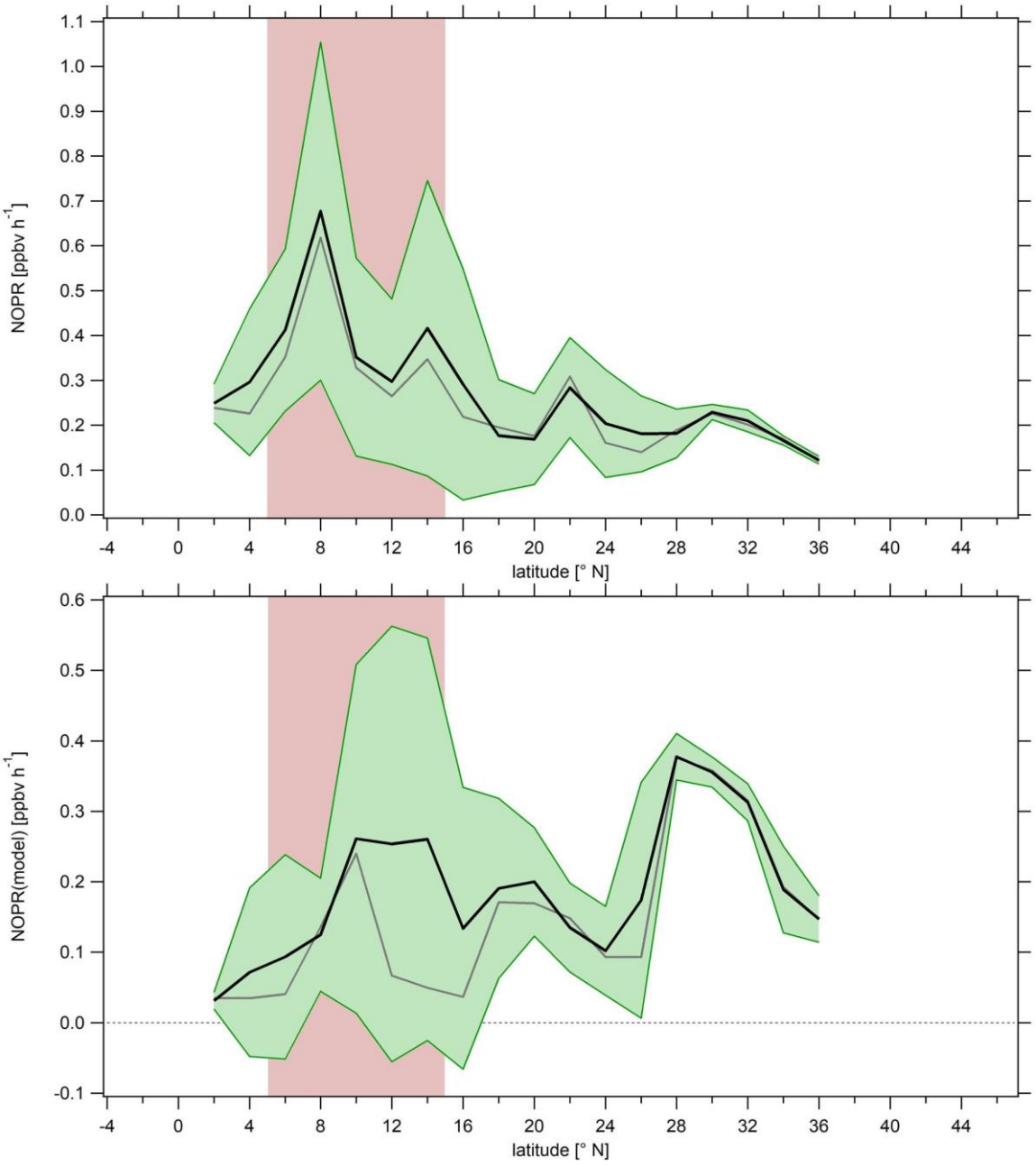

Figure S8: Latitudinal profile of NOPRs derived from measured (upper plot) and simulated (lower plot) data above 12 km at a latitudinal resolution of 2 degree. The black and grey traces represent the average and median latitudinal profile, respectively. The green background represents ±1 standard deviation of the average profile. The red box in the background indicates the supposable location of the ITCZ during August and September. The profiles were filtered for stratospheric measurements by removing data for which concurrent O_3 is > 100 ppbv.

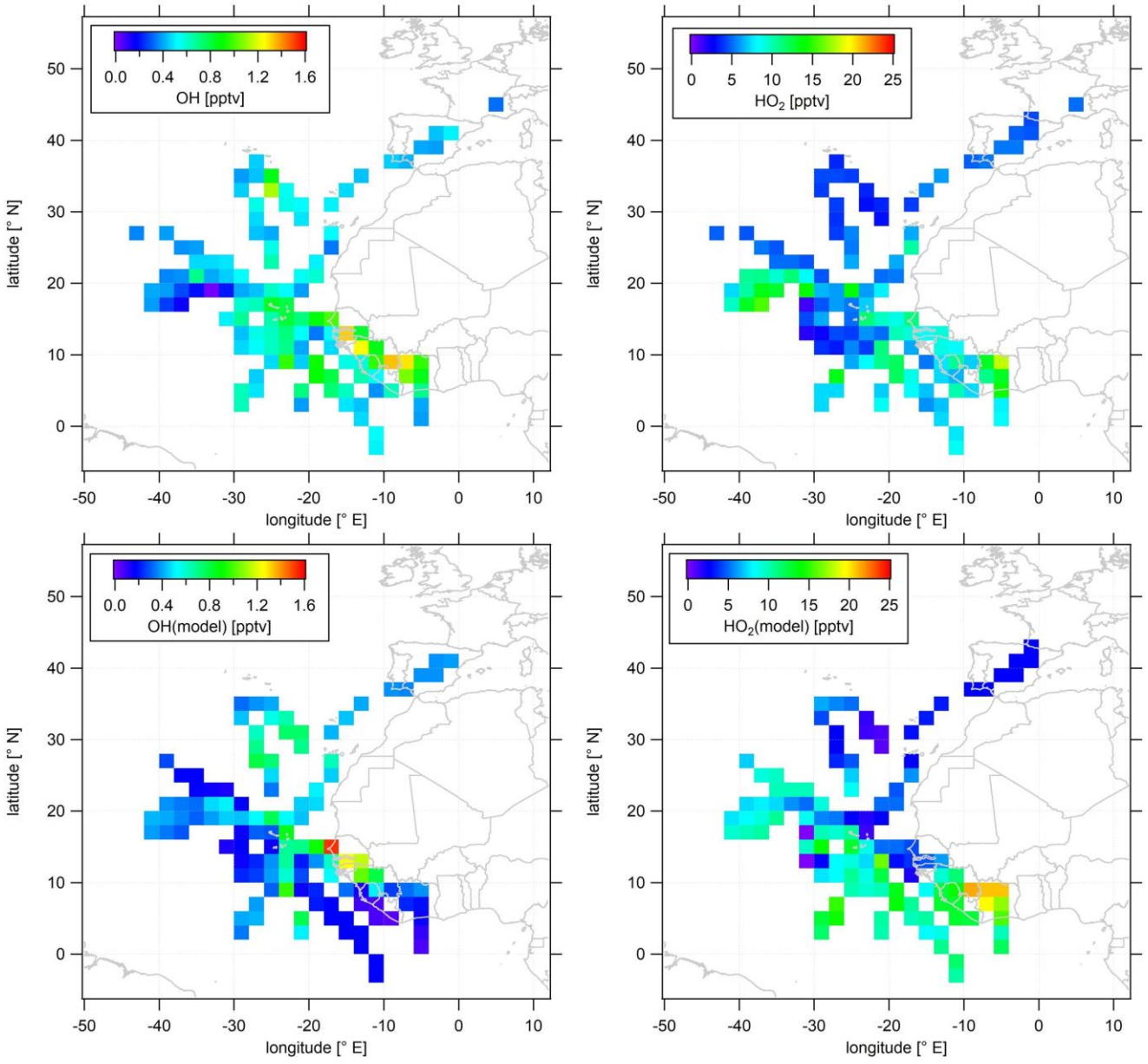

Figure S9: Color-coded spatial, tropospheric distributions of measured and simulated OH and HO_2 above 12 km during CAFE-Africa. The upper graphics show the measurements, the lower graphics show the simulations. Note that the figures are filtered for stratospheric measurements by removing data points for which concurrent O_3 is > 100 ppbv.

Table ST1: Overview of the scientific measurement flights performed during CAFE-Africa. EDMO is the international civil aviation organization (ICAO) code of the airport of the DLR facility at South Germany, GVAC the ICAO code of the airport on Sal and DGAA the ICAO code of the airport of Accra (Ghana).

Flight number	Date of the flight	Purpose/objective of the flight	Flight route
MF03	07 August 2018	ferry flight to Sal (Cape Verde Islands)	EDMO → GVAC
MF04	10 August 2018	flight south / biomass burning plume	GVAC → GVAC
MF05	12 August 2018	flight south / aged biomass burning plume	GVAC → GVAC
MF06	15 August 2018	flight north / stratospheric influence	GVAC → GVAC
MF07	17 August 2018	stack flight #1	GVAC → GVAC
MF08	19 August 2018	stack flight #2	GVAC → GVAC
MF09	22 August 2018	flight over West Africa	GVAC → DGAA
MF10	24 August 2018	flight northwest / aged biomass burning plume	GVAC → GVAC
MF11	26 August 2018	stack flight #3	GVAC → GVAC
MF12	29 August 2018	flight over the ITCZ	GVAC → GVAC
MF13	31 August 2018	flight over the ITCZ	GVAC → GVAC
MF14	02 September 2018	convective outflow of hurricane “Florence”	GVAC → GVAC
MF15	04 September 2018	flight over West Africa	GVAC → GVAC
MF16	07 September 2018	ferry flight to Oberpfaffenhofen (Germany)	GVAC → EDMO

Table ST2: List of peroxy radicals (with less than four carbon atoms) which were used to estimate RO_2 (in analogy to Tadic et al., 2020).

Species
HO_2
CH_3O_2
C_2H_5O2
$C_2H_5CO_3$
CH_3CO_3
C3DIALO2 ($C_3H_3O_4$)
CH_3CHOHO_2
$CH_3COCH_2O_2$
CH_3COCO_3
$CHOCOCH_2O_2$
$CO_2H_3CO_3$
$HCOCH_2CO_3$
$HCOCH_2O_2$
$HCOCO_3$
$HCOCOHCO_3$
$HOC_2H_4CO_3$
$HOCH_2CH_2O_2$
$HOCH_2CO_3$
$HOCH_2COCH_2O_2$
$HOCH_2O_2$
$CH_3CHO_2CH_2OH$
IC3H7O2 (isopropylperoxy radical)
NC3H7O2 (propylperoxy radical)
$NCCH_2O_2$
$NO_3CH_2CO_3$
$CH_3CHO_2CH_2ONO_2$

Table ST3: Number of data points in each NO mixing ratio bin. Note that the data coverage of the simulation is larger than that of the measurement due to gaps in the observational data.

NO mixing ratio bin	measurement	simulation
0 pptv ≤ NO < 25 pptv	140	226
25 pptv ≤ NO < 50 pptv	54	70
50 pptv ≤ NO < 75 pptv	36	40
75 pptv ≤ NO < 100 pptv	23	60
100 pptv ≤ NO < 125 pptv	50	38
125 pptv ≤ NO < 150 pptv	44	24
150 pptv ≤ NO < 175 pptv	28	7
175 pptv ≤ NO < 200 pptv	30	7
200 pptv ≤ NO < 225 pptv	21	3
225 pptv ≤ NO < 250 pptv	15	7
250 pptv ≤ NO < 275 pptv	11	3
275 pptv ≤ NO < 300 pptv	12	5
300 pptv ≤ NO < 325 pptv	11	5
325 pptv ≤ NO < 350 pptv	3	3
350 pptv ≤ NO < 375 pptv	2	6
375 pptv ≤ NO < 400 pptv	3	2
400 pptv ≤ NO < 425 pptv	1	1
425 pptv ≤ NO < 450 pptv	5	2
450 pptv ≤ NO < 475 pptv	1	3
475 pptv ≤ NO < 500 pptv	1	3

815